Entropic forces generated by grafted semiflexible polymers

Azam Gholami,[1] Jan Wilhelm,[2] and Erwin Frey[2]
[1]*Hahn-Meitner-Institut, Abteilung Theorie, Glienicker Straße 100, D-14109 Berlin, Germany*
[2]*Arnold-Sommerfeld-Center for Theoretical Physics and Center for NanoScience, Department of Physics, Ludwig-Maximilians-Universität München, Theresienstraße 37, D-80333 München, Germany*
(Received 9 March 2006; revised manuscript received 14 August 2006; published 6 October 2006)

The entropic force exerted by the Brownian fluctuations of a grafted semiflexible polymer upon a rigid smooth wall are calculated both analytically and by Monte Carlo simulations. Such forces are thought to play an important role for several cellular phenomena, in particular, the physics of actin-polymerization-driven cell motility and movement of bacteria like Listeria. In the stiff limit, where the persistence length of the polymer is larger than its contour length, we find that the entropic force shows scaling behavior. We identify the characteristic length scales and the explicit form of the scaling functions. In certain asymptotic regimes, we give simple analytical expressions which describe the full results to a very high numerical accuracy. Depending on the constraints imposed on the transverse fluctuations of the filament, there are characteristic differences in the functional form of the entropic forces. In a two-dimensional geometry, the entropic force exhibits a marked peak.

DOI: 10.1103/PhysRevE.74.041803 PACS number(s): 36.20.−r, 05.20.−y, 87.15.−v

I. INTRODUCTION

In a cellular environment, soft objects like membranes and polymers are subject to Brownian motion. As a result there are interactions between them which are entropic in origin, i.e., a consequence of constraints imposed on the Brownian fluctuations. For example, two parallel membranes repel each other entropically with a potential that falls off like a power law in the distance between them [1]. Similarly, thermally fluctuating biopolymers like F-actin and microtubules may exert entropic forces on membranes or some other obstacles; for an illustration see Fig. 1. Though due to the same thermal fluctuations, such forces have to be distinguished from forces obtained by pulling on a biopolymer [2,3]. It turns out that the force-distance curves of these two cases have no resemblance at all in a regime where thermal fluctuations play a role, which is generically the case for all cytoskeletal filaments. Both types of forces are thought to play a prominent role in cell motility and movement of pathogens like Listeria monocytogenes, that propel itself through the cytoplasm of infected cells by constructing behind it a polymerized tail of cross-linked actin filaments [4]. Similarly, in a crawling cell, the force generated from the polymerization of a collection of actin fibers is responsible for the protrusion of cell membrane, which are known as lamellipodia, filopodia, or microspikes according to their shapes [5]. It seems that polymerizing networks of actin filaments are capable of exerting significant mechanical force, which are used by eukaryotic cells and their prokaryotic pathogens to change shape or move.

In this paper, we will not enter into the debate on the particular force generating mechanism responsible for all these different types of cell motility. It seems plausible to us that a final model for a particular biological system may be a macroscopic viscoelastic model of the actin gel [6] combined with elements from a microscopic elastic Brownian ratchet (EBR) model of the growing edge of the network [7,8]. The first one is a continuum model of Listeria propulsion relying on the elastic shear stress developed by growth of the actin meshwork at the cell surface. In the EBR model, which is based on the behavior of individual actin filaments, thermal bending undulations of a semiflexible actin fiber creates the polymerization gap and the entropic force of the growing filament pushes the bacterium forward or deforms the cell membrane. It seems that a detailed analysis of the entropic forces which fluctuating stiff polymers exert on rigid walls may serve as an important input for future molecular models of force generation in cellular systems. The length of the thermally fluctuating parts of these polymers are typically 200–300 nm, which is very short compared to their persistence length $l_p \approx 15$ μm [9], such that an analysis which considers these filaments as stiff seems appropriate. For microtubules, whose persistence length ranges from 110 μm to 5 mm when L is varied between 2.6 and 47.5 μm [10], the analysis should even work better.

We consider the idealized situation illustrated in Fig. 1, where one end of a semiflexible polymer is fixed both in position and orientation to some rigid support, e.g., the dense part of an actin gel. We choose coordinates such that the grafted end is at the origin with the tangent fixed parallel to the z axis. The membrane or obstacle is considered as a rigid, smooth wall orthogonal to the x-z plane at a distance ζ from the origin. Let ϑ be the angle between the z axis and the normal $\hat{n}$ of the wall. If ζ is small enough, the wall will constrain the Brownian fluctuations of the polymer leading to an increase in free energy with respect to the unconstrained polymer. On time scales larger than the equilibration time of the grafted polymer, this results in an average force f exerted on the wall. In this paper we will calculate how the entropic force f depends on the geometric parameters ζ and ϑ, the contour length L and the persistence length ℓ_p of the polymer, and the dimensionality of the embedding space.

Polymers confined to two dimensions (2D) is a situation frequently encountered in *in vitro* experiments but also of relevance for actin filaments in the confined space of a lamellopodium. We find that in this case the entropic force shows

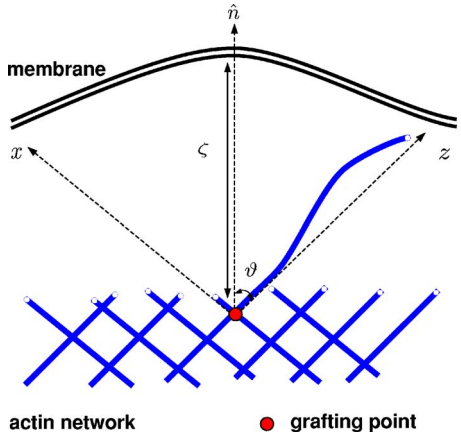

FIG. 1. (Color online) A membrane constrains the Brownian fluctuations of a semiflexible polymer grafted parallel to the z axis resulting in an entropic force on the membrane. The membrane, for simplicity, has been considered as a rigid smooth wall.

a pronounced maximum as a function of the compression of the polymer, $L-\zeta$, for a broad range of stiffness parameters $\varepsilon=L/\ell_p \leqslant 4$. The magnitude of the maximum force exceeds the value of the Euler buckling force $f_c=\frac{\pi^2}{4}\frac{\ell_p k_B T}{L^2}$ by a factor between 2 and 3. These results are quite distinct from the behavior of a polymer which is free to fluctuate in three dimensions (3D). Then the entropic force is a monotonic function of the compression and exceeds the buckling force only in the nonlinear regime for strong compressions. These qualitative results are summarized more quantitatively in the conclusions (Sec. VI).

In the branched actin network formed in lamellipodia, the Arp 2/3 complex is responsible for the nucleation of new filaments. It is found that the angle relative to the parent filament is $2\vartheta \approx 70°$ [11]. It has been asked [7,8] whether this angle corresponds to an optimal angle with respect to the entropic force generated by a fluctuating filament. Indeed, we do find that there is such an optimal angle for a homogeneous network pushing against a flat membrane (see Sec. V), but this angle is much larger, ranging in the interval $2\vartheta \in [120°, 150°]$. This angle differs from previous estimates [7,8] mainly since those were based on an incorrect value for the persistence length of actin. It would, however, be overhasty to conclude that the branching angle is not optimized for maximal force production since the simplified model in Sec. V leaves out important physics such as the polydispersity in filament length and the thermal fluctuations of the membrane.

We proceed as follows. Section II serves to introduce and discuss the various types of thermodynamic forces which can be generated by fluctuating semiflexible polymers. We arrive at the conclusion that the entropic forces discussed above are closely related to the probability distribution of the free end of the clamped polymer. In Sec. III, we start our analysis of entropic forces with a polymer grafted perpendicular to the wall. This section contains a definition of the wormlike chain model and the basic idea of our analytical calculations, which starting from the tip distribution calculates the restricted free energy and the entropic force. The analysis is complemented by Monte Carlo (MC) simulations, which both show the range of validity of the analytical results and the crossover from semiflexible to Gaussian chains. Details of the calculations are deferred to the Appendixes A, B, and C. Section IV treats the technically more complicated case of a polymer inclined at an angle ϑ with respect to the wall. Here, we obtain the entropic forces analytically up to the numerical evaluation of some integrals. For some asymptotic cases, explicit analytical formula are again obtained. The MC simulations in this chapter are restricted to a parameter range which is close to the stiff limit and mainly serve the purpose to define the range of applicability of the analytical results. In Sec. V, we take the polymerization kinetics of the filaments into account and show that there is an optimal angle at which the polymerization velocity is maximum. Finally, in the conclusion, we give a discussion of our main results.

II. ENTROPIC FORCES AND PROBABILITY DENSITIES

According to the *wormlike chain model* [12,13], the elastic energy of a given configuration $\mathbf{r}(s)$, parametrized in terms of the arc length $s \in [0,L]$, is given by

$$\beta H = \frac{\ell_p}{2}\int_0^L ds \left(\frac{\partial \mathbf{t}(s)}{\partial s}\right)^2. \tag{1}$$

Here $\mathbf{t}(s)=\partial \mathbf{r}(s)/\partial s \equiv \dot{\mathbf{r}}(s)$ is the local tangent to the contour $\mathbf{r}(s)$, $\ell_p=\kappa/k_B T$ is the persistence length with κ the polymer's bending modulus, and $\beta=1/k_B T$. As the polymer is considered to be inextensible, we have $|\mathbf{t}(s)|=1$, for all s, i.e., the tangent vectors are restricted to the unit sphere.

In a cellular environment, biopolymers are flexed by Brownian motion, i.e., they exhibit thermal fluctuations in their shape. This makes for a rich mechanic response genuinely different from its classical analogue, a rigid beam. Consider a polymer whose position (not its orientation) is fixed at one end and one is pulling on its other end, a typical situation encountered in an experiment using optical or magnetic tweezers. Then there is no unique force-distance relation. It actually matters whether one pulls at constant force f and measures the resulting average distance $\langle r\rangle(f)$ or vice versa. Results for the constant force ensemble are thoroughly discussed in Ref. [2]. In a constant distance ensemble, the probability density distribution of the end-to-end distance $P(r)$ provides the necessary information [14]. It defines a free energy $F(r)=-k_B T \ln P(r)$ from which the average force may be derived by differentiation, $\langle f\rangle(r)=-\partial F(r)/\partial r$ [15].

Here, we are interested in the force a fluctuating filament exerts on a rigid obstacle which is fixed in its position [16]. The polymer's end facing the obstacle is considered as free to fluctuate and only its proximal end is fixed in position and orientation; see Fig. 1. Since there are no direct forces between polymer and obstacle the force exerted on the wall is solely due to the steric constraints imposed on the filament. This suggests to use the term "entropic forces," frequently used in analogous physical situations [17]. However, this should not leave the reader with the wrong impression that there are different physical origins for entropic forces and

those discussed in the preceding paragraph. It is merely the type of "boundary condition" imposed on the thermal fluctuations which leads to their (drastically) different character.

For getting acquainted with the problem, let us consider the simplest case, a grafted polymer whose one end and tangent is fixed such that it is oriented perpendicular to a smooth wall (Fig. 1 with $\vartheta=0$). The presence of the wall allows only for those polymer configurations which are entirely in the half-space to the left of the wall. Since we are mostly interested in stiff polymers (which have a low probability for back-turns), this restriction may be approximated as a constraint solely on the position of the polymer tip facing the wall, $r_z(L) \leqslant \zeta$; later in Sec. IV C we will show some simulation data going beyond this approximation.

To derive the average force acting on the wall, we consider a wall potential $U[\zeta - r_z(L)]$ for the free polymer tip, which at the end of the calculation will be reduced to a hard wall potential. For now, picture a steep potential which rises rapidly for $r_z(L) \to \zeta$. Then, the ensemble average for the force that the polymer tip exerts perpendicular to the wall reads

$$\langle f_\parallel \rangle(\zeta) = \frac{1}{\mathcal{Z}_\parallel(\zeta)} \int \mathcal{D}[\mathbf{r}(s)] e^{-\beta(H+U)} \frac{\partial U}{\partial r_z(L)}. \tag{2}$$

Here the partition sum

$$\mathcal{Z}_\parallel(\zeta) = \int \mathcal{D}[\mathbf{r}(s)] e^{-\beta(H+U)} \tag{3}$$

is a path integral over all polymer configurations compatible with the boundary conditions imposed on the distal and free end of the grafted polymer, where the measure is taken such that the partition sum without a constraining wall ($U=0$) is normalized to 1. This is now a thermodynamic force. In an actual experiment, it is obtained by a time average with an averaging time much larger than the equilibration time for the grafted polymer. This force would also be measured in an experiment where a large number of independent and identical polymers push against the same wall.

Since the wall potential depends only on the difference between the position of the polymer tip and the wall, we may rewrite the entropic force in (2) as

$$\langle f_\parallel \rangle(\zeta) = k_B T \frac{\partial}{\partial \zeta} \ln \mathcal{Z}_\parallel(\zeta). \tag{4}$$

Upon defining a free energy of the confined polymer as

$$\mathcal{F}_\parallel(\zeta) = -k_B T \ln \mathcal{Z}_\parallel(\zeta), \tag{5}$$

the entropic forces again reads as a spatial derivative of a free energy

$$\langle f_\parallel \rangle(\zeta) = -\frac{\partial}{\partial \zeta} \mathcal{F}_\parallel(\zeta). \tag{6}$$

The physical interpretation of this free energy becomes clear as one goes to the hard wall limit. Then the partition function reduces to

$$\mathcal{Z}_\parallel(\zeta) = \int \mathcal{D}[\mathbf{r}(s)] \Theta(\zeta - r_z(L)) e^{-\beta H} =: \langle \Theta(\zeta - r_z(L)) \rangle_0, \tag{7}$$

where the subscript 0 indicates that the average is now taken with respect to the bending Hamiltonian only. The Θ function, defined such that $\Theta(x)=1$ for $x>0$ and zero elsewhere, indicates that only those configurations are counted with the position of the polymer tip to the left of the wall. Hence, as for the fixed distance ensemble in a pulling experiment, the free energy results from a quantity measuring the number of configurations obeying the imposed constraint, where each configuration is weighted by a Boltzmann factor for the bending energy.

It is useful to rewrite the partition function as

$$\mathcal{Z}_\parallel(\zeta) = \int_{-L}^{L} dz \Theta(\zeta - z) \langle \delta(z - r_z(L)) \rangle_0 = \int_{-L}^{\zeta} dz P_\parallel(z), \tag{8}$$

where $P_\parallel(z) = \langle \delta(z - r_z(L)) \rangle_0$ is the probability density to find the z coordinate of the polymer's free end at z irrespective of its transverse coordinates. It identifies the restricted partition sum as the cumulative distribution function corresponding to the probability density $P_\parallel(z)$. One may then write the entropic force in the alternative form

$$\langle f_\parallel \rangle(\zeta) = k_B T \frac{P_\parallel(\zeta)}{\mathcal{Z}_\parallel(\zeta)}. \tag{9}$$

Upon multiplying this formula by $d\zeta$, it may be interpreted as follows. The work done on the wall upon displacing it by an infinitesimal distance $d\zeta$ equals the thermal energy scale $k_B T$ times a conditional probability $P_{\text{left}}(\zeta) d\zeta = P_\parallel(\zeta) d\zeta / \mathcal{Z}_\parallel(\zeta)$, which measures the probability that the position of the polymer tip is within a distance $d\zeta$ from the wall given that the polymer is in the left half-space.

Since the probability density for the position of the polymer tip $P(\mathbf{x}, z)$ is actually a function of the position perpendicular and transverse to the wall, (9) immediately suggests that one could define a *local* entropic pressure. Indeed, upon generalizing the above arguments, one may write

$$\begin{aligned} p(\mathbf{x}, \zeta) &= \frac{-1}{\mathcal{Z}_\parallel(\zeta)} \int \mathcal{D}[\mathbf{r}] \frac{\partial U}{\partial \zeta} \delta(\mathbf{x} - \mathbf{r}_\perp(L)) e^{-\beta(H+U)} \\ &= \frac{k_B T}{\mathcal{Z}_\parallel(\zeta)} \frac{\partial}{\partial \zeta} \langle \Theta(\zeta - r_z(L)) \delta(\mathbf{x} - \mathbf{r}_\perp(L)) \rangle_0 \\ &= k_B T \frac{P(\mathbf{x}, \zeta)}{\mathcal{Z}_\parallel(\zeta)} \end{aligned} \tag{10}$$

for the entropic pressure, i.e., the force per unit area exerted locally at $\mathbf{x}$ on the wall. Again, the entropic force is given by the thermal energy scale times a conditional probability density, which now measures the probability of finding the polymer tip at a particular site $\mathbf{x}$ on the wall conditioned on the polymer configuration being to the left of the wall. Pictorially, one may say that the local pressure is given by $k_B T$ times the number of "collisions" of the polymer with the

wall per unit area, a reasoning which is frequently used in scaling analyses.

The total force is obtained by integrating over this local pressure, $\langle f_\parallel\rangle(\zeta)=\int d\mathbf{x}p(\mathbf{x},\zeta)$. In addition, one may now also define an entropic torque as has recently been done for a rigid rod facing a planar wall [18]; we leave this issue for future investigations.

Generalizing the above ideas suggests to introduce an effective local free energy per unit area as

$$\mathcal{F}(\mathbf{x},\zeta)=-k_BT\int^{\zeta}dz\frac{P(\mathbf{x},z)}{\mathcal{Z}_\parallel(z)}, \tag{11}$$

which is useful in applications where the obstacle is actually not rigid but soft with some internal elasticity, e.g., a membrane whose dynamics is much slower than the equilibration time of the polymer. Then the elastic energy describing membrane bending and the above effective free energy may just be added to describe the combined system. Of course, such a description fails if time scales for the dynamics of both soft objects are comparable.

Our main conclusion in this section is that entropic forces generated by a grafted stiff polymer can be reduced to the calculation of the probability distribution of the polymer tip. For a polymer constrained to two dimensions, the distribution function has been found to show quite interesting behavior such as bimodality in the transverse displacement of the free end [19]. This pronounced feature of the distribution function has recently been rationalized upon exploiting an interesting analogy to a random walker in shear flow [20].

III. POLYMER ORTHOGONAL TO A WALL

In this section, we are going to calculate the entropic force generated by a grafted polymer whose orientation is on average perpendicular to the wall. It illustrates the basic idea of our analytical calculations for the simplest geometry.

A. Weakly bending limit: mode analysis

In evaluating the distribution function analytically, we restrict ourselves to the limit of a *weakly bending filament*. In other words, we consider the persistence length ℓ_p to be large enough compared to the total contour length L, such that the statistical weight of configurations with small sharp bends will be negligible. The key small dimensionless quantity will be the *stiffness parameter*

$$\varepsilon=L/\ell_p \tag{12}$$

and we will refer to the weakly bending limit also as the *stiff limit*.

For small ε, the transverse components $t_x(s)$ and $t_y(s)$ of the tangent vector $\mathbf{t}(s)$ will be small for all s. The condition $|\mathbf{t}(s)|=1$ would suggest a parameterization of $\mathbf{t}(s)$ in terms of polar coordinates or Euler angles. Such a parametrization, however, becomes quite cumbersome in the present case where the embedding into an external space matters due to the steric constraints imposed by the wall. It is much more convenient to use a Monge-like parametrization,

$$\mathbf{t}=\frac{1}{\sqrt{1+a_x^2+a_y^2}}\begin{pmatrix}a_x\\a_y\\1\end{pmatrix}, \tag{13}$$

where we dropped all arguments s for brevity; the generalization to d spatial dimensions is obvious.

The boundary conditions at the ends of the polymer are

$$\mathbf{t}(0)=(0,0,1)^T \quad \text{(clamped end)}, \tag{14a}$$

$$\dot{\mathbf{t}}(L)=(0,0,0)^T \quad \text{(free end)}. \tag{14b}$$

This translates into $\mathbf{a}(0)=[a_x(0),a_y(0)]^T=(0,0)^T$ and $\dot{\mathbf{a}}(L)=[\dot{a}_x(L),\dot{a}_y(L)]^T=(0,0)^T$. We thus can choose a Fourier representation or in other words a *normal mode decomposition*

$$a_x(s)=\sum_{k=1}^{\infty}a_{x,k}\sin\left(\lambda_k\frac{s}{L}\right) \tag{15}$$

with eigenvalues

$$\lambda_k=\frac{\pi}{2}(2k-1), \tag{16}$$

and Fourier (normal mode) amplitudes

$$a_{x,k}=\frac{2}{L}\int_0^L dsa_x(s)\sin\left(\lambda_k\frac{s}{L}\right), \tag{17}$$

and similar for $a_y(s)$. To second order in the Fourier amplitudes, the location of the endpoint along the z axis reads

$$r_z(L)=\int_0^L dst_z(s)\approx L-\frac{1}{2}\int_0^L ds[a_x^2(s)+a_y^2(s)]$$
$$=L-\frac{L}{4}\sum_{k=1}^{\infty}(a_{x,k}^2+a_{y,k}^2). \tag{18}$$

Similarly, we find for the Hamiltonian to second order

$$\beta H\approx\frac{\ell_p}{4L}\sum_{k=1}^{\infty}\lambda_k^2(a_{x,k}^2+a_{y,k}^2). \tag{19}$$

B. Moment generating function

To calculate the probability density function $P_\parallel(z)$, we follow a procedure outlined in Ref. [14] and consider the moment generating function

$$\mathcal{P}_\parallel(f):=\langle e^{-f[L-r_z(L)]}\rangle_0$$
$$=\int_{-L}^{L}dze^{-f(L-z)}P_\parallel(z)$$
$$=\int_0^{2L}d\rho e^{-f\rho}P_\parallel(L-\rho). \tag{20}$$

Note that thermal averages must be evaluated using the bare elastic free energy (1). Since for stiff chains configurations

with large values for the stored length ("compression") $\rho = L - z$ are rather unlikely, we can extend the upper boundary of the integral in the last line of the preceding equation to infinity. This allows us to write the moment generating function as the Laplace transform of the distribution function $P_\parallel(z)$,

$$\mathcal{P}_\parallel(f) = \int_0^\infty d\rho e^{-f\rho} P_\parallel(L-\rho). \tag{21}$$

For $f=0$, the latter equation reduces to the normalization condition of the probability density function $P_\parallel(z)$ such that $\mathcal{P}_\parallel(0)=1$.

Combining Eqs. (18)–(20), the moment generating function can be rewritten into the following path integral form:

$$\mathcal{P}_\parallel(f) = \int \mathcal{D}[\mathbf{a}(s)] \exp\left(-\frac{1}{2}\int_0^L ds(\ell_p \dot{\mathbf{a}}^2 + f\mathbf{a}^2)\right) \tag{22}$$

with the boundary conditions given by (14). This path integral is easily evaluated upon using the Fourier representation of the transverse tangent fields Eq. (15), and noting that to harmonic order fluctuations in all transverse directions are statistically independent. We find in d spatial dimensions

$$\mathcal{P}_\parallel(f) = \left\{ \int \prod_{k=1}^{\infty} \frac{da_k}{\mathcal{N}} \exp\left[-\frac{1}{4}\left(\frac{\lambda_k^2 \ell_p}{L} + fL\right) a_k^2\right] \right\}^{(d-1)}$$
$$= \prod_{k=1}^{\infty} \left(1 + \frac{fL^2}{\ell_p \lambda_k^2}\right)^{-(d-1)/2}, \tag{23}$$

where the normalization factor $\mathcal{N}$ of the path integral was chosen such that $\mathcal{P}_\parallel(0)=1$. If $f \in \mathbb{R}_+$ the product may be rewritten as [22]

$$\mathcal{P}_\parallel(f) = \left(\cosh \sqrt{\frac{fL^2}{\ell_p}}\right)^{-(1/2)(d-1)}. \tag{24}$$

Note that the moment generating function, which also depends on the length scales L and ℓ_p, has the scaling form

$$\mathcal{P}_\parallel(f, L, \ell_p) = \tilde{\mathcal{P}}_\parallel(fL_\parallel), \tag{25}$$

where we have defined the characteristic *longitudinal length scale*

$$L_\parallel := \frac{L^2}{\ell_p}. \tag{26}$$

The formulas in (23) and (24) are the basis for all subsequent calculations in this section, which are basically different forms of performing the inverse Laplace transform.

For future reference and comparison with the entropic forces, we close this section with a discussion of the force-extension relation in the fixed force ensemble. It simply follows as the first moment of the moment generating function

$$\langle r_z(L)\rangle_f = L + \frac{\partial \ln \mathcal{P}_\parallel(f)}{\partial f} = L\left(1 - \frac{L(d-1)}{4\ell_p} \frac{\tanh\sqrt{fL_\parallel}}{\sqrt{fL_\parallel}}\right), \tag{27}$$

where f is the external force in units of the thermal energy k_BT. In the limit of small external forces, this reduces to

$$\langle r_z(L)\rangle_f = L\left[1 - \frac{d-1}{4}\frac{L}{\ell_p} + \frac{d-1}{12}\left(\frac{L}{\ell_p}\right)^2 fL\right], \tag{28}$$

which identifies $L_\parallel$ as $4/(d-1)$ times the equilibrium stored length due to thermal fluctuations. We also recover the effective linear spring coefficient $k_\parallel = 12\kappa^2/(d-1)k_BTL^4$, which was previously calculated in Ref. [23]. For strong stretching forces the extension saturates asymptotically as

$$\langle r_z(L)\rangle_f = L\left(1 - \frac{L(d-1)}{4\ell_p\sqrt{fL_\parallel}}\right). \tag{29}$$

In the limit of large compressional forces, the weakly bending rod approximation breaks down and one must use different approaches to evaluate the force-extension relation [15].

C. Probability density for the position of the polymer tip: Analytical and MC results in 3D

We now return to the distribution function and the resulting entropic forces. Upon performing the inverse Laplace transform one gets (for details of the calculations see Appendix A 1)

$$P_\parallel(z) = \frac{2}{L_\parallel}\sum_{k=1}^{\infty} (-1)^{k+1}\lambda_k \exp\left(-\lambda_k^2 \frac{L-z}{L_\parallel}\right). \tag{30}$$

Inspection of Eq. (33) immediately tells us that it can be written in scaling form

$$P_\parallel(z, L, \ell_p) = L_\parallel^{-1} \tilde{P}_\parallel(\tilde{\rho}), \tag{31}$$

where we have made the dependence of the probability density on L and ℓ_p explicit and introduced the scaling variable

$$\tilde{\rho} = \frac{L-z}{L_\parallel} \tag{32}$$

measuring the compression of the filament in units of $L_\parallel$. This implies that data for the probability density of the polymer tip can be rescaled to fall on a *scaling function* $\tilde{P}_\parallel(\tilde{\rho})$, shown as the solid curve in Fig. 2. Of course, since the analytical calculations are based on the mode analysis in the weakly bending limit, such a universal scaling curve is obtained only for small enough stiffness parameters ε.

The probability density is strongly peaked towards full stretching, $\tilde{\rho} \to 0$, and falls off exponentially for large $\tilde{\rho}$, such that for $\tilde{\rho} \geqslant 0.3$,

$$\tilde{P}_\parallel^{>}(\tilde{\rho}) = \pi \exp\left(-\tfrac{1}{4}\pi^2\tilde{\rho}\right) \tag{33}$$

is already an excellent approximation. The series expansion given by (30) converges well for all values of z well below L, but its convergence properties become increasingly worse if

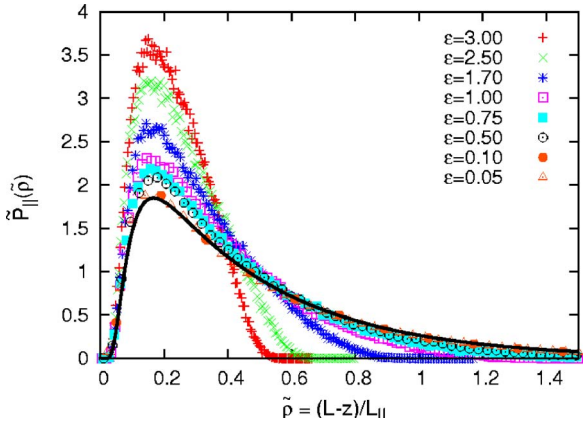

FIG. 2. (Color online) Scaling function $\tilde{P}_{\parallel}(\tilde{\rho})$ (solid line) in 3D for the probability density to find the free end of a grafted semiflexible polymer in a plane defined by $r_z(L)=z$ or equivalently with a reduced stored length $\tilde{\rho}$. For comparison, MC data are given for a series of stiffness parameters $\varepsilon=L/\ell_p$ indicated in the graph. Deviations from the scaling curve in the stiff limit become significant for $\varepsilon \geqslant 0.5$.

z approaches L. As detailed in Appendix A 2, one may also derive an alternative series representation of the tip distribution function which converges well close to full stretching

$$\tilde{P}_{\parallel}(\tilde{\rho}) = \sum_{l=0}^{\infty} (-1)^l \frac{2l+1}{\sqrt{\pi\tilde{\rho}^3}} \exp\left(-\frac{\left(l+\frac{1}{2}\right)^2}{\tilde{\rho}}\right). \tag{34}$$

Already the first term of (34),

$$\tilde{P}_{\parallel}^{<}(\tilde{\rho}) = \frac{1}{\sqrt{\pi\tilde{\rho}^3}} \exp\left(-\frac{1}{4\tilde{\rho}}\right) \tag{35}$$

gives an excellent fit for $\tilde{\rho} \leqslant 0.3$. In particular, it captures the main feature of the distribution function, namely its maximum is close to full stretching. The same approximate expression may also be obtained by evaluating the inverse Laplace transform using the method of steepest descent; see Appendix B. The asymptotic results given in (35) and (33) taken together give a representation of the scaling curve to a very high numerical accuracy. They are the analogues of the results found in Ref. [14] for a freely fluctuating filament; see also Ref. [15].

The MC data shown in Fig. 2 have been obtained by using a standard algorithm for a discretized wormlike chain, similar to the one described in Ref. [14]. As expected, the MC results agree very well with the analytical calculations for small values of ε. From Fig. 2 we can read off that the asymptotic stiff scaling regime remains valid up to stiffness parameters $\varepsilon \approx 0.1$; even for $\varepsilon=0.5$ the shape of the scaling function resembles the MC data quite closely. As the polymer becomes more flexible, the shape asymptotically becomes Gaussian; for $\varepsilon=3$ a skew is still noticeable. Note that in the parameter range given in Fig. 2, the width of the rescaled probability densities stays approximately the same and is hence well characterized by the longitudinal scale $L_{\parallel}$.

D. Confinement free energy and entropic forces: 3D

Now we are in a position to calculate the restricted partition sum (cumulative probability distribution) $\mathcal{Z}_{\parallel}(\zeta) = \int_{-L}^{\zeta} dz P_{\parallel}(z)$ by (formally) integrating the series expansion of (30) term by term. This gives

$$\mathcal{Z}_{\parallel}(\zeta) = 1 - \int_{\zeta}^{L} dz P_{\parallel}(z) = 1 - 2\sum_{k=1}^{\infty} (-1)^{k+1} \lambda_k^{-1} (1 - e^{-\lambda_k^2 (L-\zeta)/L_{\parallel}})$$

$$= 2\sum_{k=1}^{\infty} (-1)^{k+1} \lambda_k^{-1} e^{-\lambda_k^2 (L-\zeta)/L_{\parallel}}, \tag{36}$$

where in the first line we used the normalization of $P_{\parallel}(z)$ and in the last line the identity [21]

$$\sum_{k=1}^{\infty} (-1)^{k+1} \frac{1}{2k-1} = \frac{\pi}{4}. \tag{37}$$

The series expansion in (36) converges well for all values of ζ well below L. Alternatively, one may start from (34) and derive

$$\mathcal{Z}_{\parallel}(\zeta) = 1 + 2\sum_{k=1}^{\infty} (-1)^k \operatorname{erfc}\left(\frac{\lambda_k/\pi}{\sqrt{(L-\zeta)/L_{\parallel}}}\right), \tag{38}$$

which is well behaved for ζ close to L, and dominated by its first term. A second method to obtain (38) can be found in Appendix C.

From both series expansions, it is evident that the restricted partition sum has the scaling property

$$\mathcal{Z}_{\parallel}(\zeta, L, \ell_p) = \tilde{\mathcal{Z}}_{\parallel}(\tilde{\eta}), \tag{39}$$

where we have introduced the scaling variable

$$\tilde{\eta} = \frac{L-\zeta}{L_{\parallel}}, \tag{40}$$

which measures the minimal stored length (compression) $\eta = L - \zeta$ of the filament in units of $L_{\parallel}$. The confinement free energy, $\tilde{\mathcal{F}}_{\parallel}(\tilde{\eta}) = -k_B T \ln \tilde{\mathcal{Z}}_{\parallel}(\tilde{\eta})$, corresponding to this partition function is shown in Fig. 3. Again, the universal scaling function describes the MC data well for $\varepsilon \leqslant 0.1$. Note that for all values of $\tilde{\eta}$ and the stiffness parameter ε, the free energy is convex. This will turn out to be an important feature which distinguishes the 3D and 2D case.

Upon using (9) for the entropic force we find

$$f_{\parallel}(\zeta) = \frac{k_B T}{L_{\parallel}} \frac{\tilde{P}_{\parallel}(\tilde{\eta})}{\tilde{\mathcal{Z}}_{\parallel}(\tilde{\eta})} \tag{41}$$

which immediately shows its scaling behavior and identifies $k_B T/L_{\parallel}$ as the characteristic force scale. It is up to a prefactor identical to the critical force

$$f_c = \frac{\pi^2 \kappa}{4L^2} = \frac{\pi^2}{4} \frac{k_B T}{L_{\parallel}} \tag{42}$$

for the buckling instability of a classical Euler-Bernoulli beam [24]. It suggests to rewrite the entropic force as

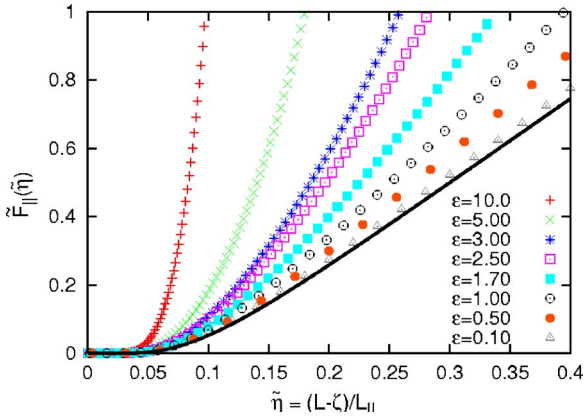

FIG. 3. (Color online) Confinement free energy $\tilde{\mathcal{F}}_{\|}(\tilde{\eta})$ of a grafted polymer constrained by a rigid wall in 3D as a function of the reduced minimal stored length $\tilde{\eta}=(L-\zeta)/L_{\|}$. The solid line gives the scaling function obtained in the limit of a weakly bending rod. Symbols represent MC data for different values of the stiffness parameter ε as indicated in the graph.

$$f_{\|}(\zeta,L,\ell_p) = f_c \tilde{f}_{\|}(\tilde{\eta}), \tag{43}$$

with the scaling function

$$\tilde{f}_{\|}(\tilde{\eta}) := \frac{4}{\pi^2}\frac{\tilde{P}_{\|}(\tilde{\eta})}{\tilde{\mathcal{Z}}_{\|}(\tilde{\eta})}. \tag{44}$$

The analytical result for the scaling function $\tilde{f}_{\|}(\tilde{\eta})$, shown as the solid curve in Fig. 4, has several characteristic features. First of all, it is always monotonically increasing since the free energy is convex. For $\tilde{\eta}\gtrapprox 0.4$, the scaling function is $\tilde{f}_{\|}\approx 1$ corresponding to $f_{\|}\approx f_c$, i.e., a vanishing contribution of thermal fluctuations to the force. For smaller $\tilde{\eta}$, corresponding to larger distances ζ between the wall and the grafted end of the polymer, fluctuations reduce the force exerted on the wall by effectively shortening the polymer. For

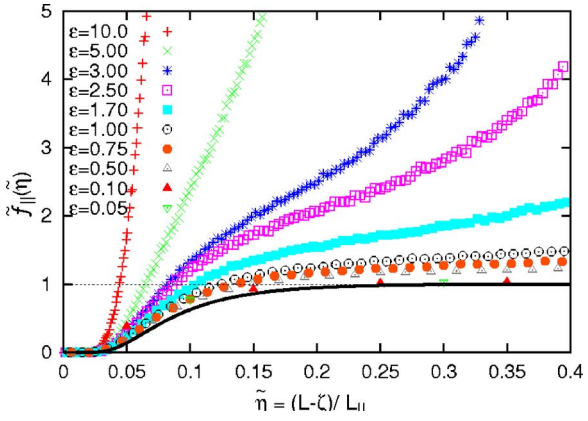

FIG. 4. (Color online) Scaling function $\tilde{f}_{\|}(\tilde{\eta})$ for the entropic force exerted on a wall at a distance ζ from the grafted end as a function of the scaling variable $\tilde{\eta}=(L-\zeta)/L_{\|}$. Symbols represent MC data for different stiffness parameters ε, as indicated in the graph. Entropic force is a monotonically increasing function of $\tilde{\eta}$.

$\zeta\to L$ (respectively, $\tilde{\eta}=0$), the probability of the polymer to contact the wall becomes smaller and smaller until finally for $\zeta=L$ only one configuration, namely the completely straight one, has $r_z(L)=L$. Hence the force must vanish for all $\zeta\geqslant L$ (respectively, $\tilde{\eta}\leqslant 0$).

We have learned already in Sec. III C that there are excellent approximations to the scaling function for the probability density of the free polymer end for small values of the reduced stored length (35). In the same way, the first term of (38) is an excellent approximation to the infinite series for $\tilde{\eta}\lessapprox 0.2$. Thus, we may write for the scaling function of the entropic force

$$\tilde{f}_{\|}^{<}(\tilde{\eta}) = \frac{4e^{-1/4\,\tilde{\eta}}}{\pi^{5/2}\tilde{\eta}^{3/2}[1-2\,\mathrm{erfc}(1/2\sqrt{\tilde{\eta}})]}, \tag{45}$$

which already describes most of the nontrivial shape of the scaling function. For $\tilde{\eta}\gtrsim 0.2$, it suffices to high accuracy to use the first two terms of (36), which gives

$$\tilde{f}_{\|}^{>}(\tilde{\eta}) = \frac{1-3e^{-2\pi^2\tilde{\eta}}}{1-\frac{1}{3}e^{-2\pi^2\tilde{\eta}}}. \tag{46}$$

Upon inspection of (41), one may interpret the functional form of the entropic force as due to two effects. In the numerator, we have the probability density for the position of the free end at the wall. This function shows a pronounced peak as one decreases the distance ζ (respectively, increases the scaling variable $\tilde{\eta}$). At the same time, the denominator, the cumulative distribution function, decreases by decreasing ζ. It is now a matter of how fast these changes occur and what the ensuing shape of the scaling function for the entropic force will be. In the present case of a polymer in 3D, the decrease in the cumulative distribution function seems to be fast enough to compensate the maximum in the probability density of the free polymer end such that the entropic force becomes a monotonically increasing function of $\tilde{\eta}$.

From Fig. 4, one observes that the universal scaling curve is a lower bound to the MC data for all values of the stiffness parameter ε. For fixed ε, the entropic force always increases monotonically with increasing compression; for intermediate values $\varepsilon\approx 2.5$ there is a pronounced change in curvature at $\tilde{\eta}\approx 0.25$. For strong compression the results asymptote to the mechanical limit ($k_BT=0$). This limit is not correctly reproduced within the harmonic approximation which gives

$$f_{\mathrm{mech}}(\zeta) = f_c\Theta(L-\zeta), \tag{47}$$

whereas the exact force-extension curve is a monotonous function in ζ that is somewhat larger than f_c for $\zeta<L$ and tends to f_c for $\zeta\to L$.

One might finally ask, whether these entropic forces $f_{\|}(\zeta)$ are related to the force extension relation discussed in Sec. III B, $\langle r_z(L)\rangle_f-\langle r_z(L)\rangle_0=k_{\|}^{-1}f+O(f^2)$ with $k_{\|}=6\kappa^2/k_BTL^4$ [23]. Rewriting these linear response result in scaling form we find

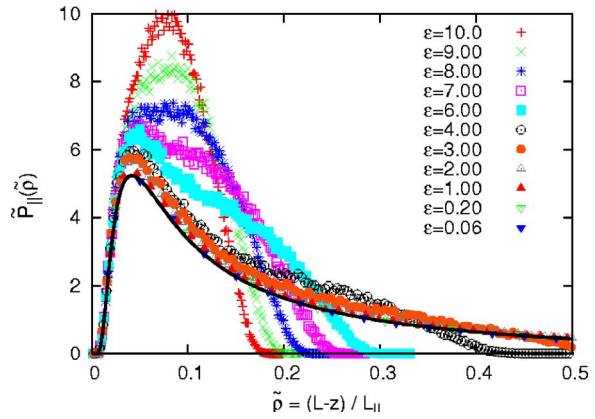

FIG. 5. (Color online) Probability density $\tilde{P}_{\|}(\tilde{\rho})$ of the free end of a grafted semiflexible polymer in 2D as a function of $\tilde{\rho}$ (solid curve). Symbols represent MC data for different stiffness parameters, as indicated in the graph. MC data deviate from universal curve as ϵ increases.

$$\frac{f}{f_c} = \frac{24}{\pi^2}\left(\tilde{\eta} - \frac{1}{2}\right). \tag{48}$$

Comparing this with Fig. 4, we see that the linear response result does not contain any information about the situation under investigation here. To the contrary, the initial rise of the force when ζ becomes slightly smaller than L is highly nonlinear [see Eq. (45)].

E. Distribution function and entropic forces: 2D

Since in some important physiological situations like the leading edge of a crawling cell, polymer is essentially confined to fluctuate in 2D, it is important to look at the 2D problem more precisely. Analogous to the preceding section, the tip distribution function of a polymer confined to 2D, e.g., by two parallel glass plates, obeys a scaling law in the stiff limit

$$P_{\|}(z,L,\ell_p) = L_{\|}^{-1}\tilde{P}_{\|}(\tilde{\rho}). \tag{49}$$

The scaling function may again be represented in terms of series expansions (see Appendix A 2). A series which converges well for small values of $\tilde{\rho}$ reads

$$\tilde{P}_{\|}(\tilde{\rho}) = \sum_{l=0}^{\infty}\binom{-\frac{1}{2}}{l}\frac{2l+\frac{1}{2}}{\sqrt{2\pi}\tilde{\rho}^{3/2}}\exp\left(-\frac{\left(l+\frac{1}{4}\right)^2}{\tilde{\rho}}\right); \tag{50}$$

for an explicit formula for the binomial coefficient in (50) see (A17). The scaling function, shown as the solid curve in Fig. 5, has an overall shape which is quite similar to 3D with a pronounced maximum close to full stretching. The series approximations may again give useful approximate expressions for the shape. In the proximity of full stretching, the series given by (50) converges very fast such that already the first term

$$\tilde{P}_{\|}^{<}(\tilde{\rho}) = \frac{1}{\sqrt{8\pi}\tilde{\rho}^{3/2}}\exp\left(-\frac{1}{16\tilde{\rho}}\right) \tag{51}$$

is an excellent approximation for the whole series at least for $\tilde{\rho} \leqslant 0.3$. As in 3D, a saddle point approximation also gives (51) (see Appendix B). Alternatively, as shown in Appendix A 2, one may derive a series expansion which converges well in the strong compression limit; see (A11). For $\tilde{\rho} \lessapprox 0.3$, it suffices to use the first term of this sum only which reads

$$\tilde{P}_{\|}^{>}(\tilde{\rho}) = \frac{\pi e^{-\pi^2\tilde{\rho}/4}}{2\sqrt{2}}(1 + 1.5e^{-5\pi^2\tilde{\rho}/16} + 2e^{-12\pi^2\tilde{\rho}/16} + 2.5e^{-21\pi^2\tilde{\rho}/16} + 3e^{-32\pi^2\tilde{\rho}/16}). \tag{52}$$

Upon increasing the stiffness parameter, the rescaled probability distribution deviates from the scaling function in the semiflexible limit and approaches a Gaussian distribution. In contrast to 3D, there is an intermediate parameter regime in the stiffness parameter where $\tilde{P}_{\|}(\tilde{\rho})$ exhibits a marked shoulder. This feature of the distribution function has recently been identified and explained in terms of an interesting analogy with the physics of a random walker in shear flow [20].

Upon integrating (50) from $-L$ to ζ, one obtains for the restricted partition sum

$$\mathcal{Z}_{\|}(\zeta) = 1 - \sqrt{2}\sum_{k=0}^{\infty}\frac{(-1)^k(2k-1)!!}{2^k k!}\operatorname{erfc}\left(\frac{\lambda_{2k+1}}{2\pi\sqrt{\tilde{\eta}}}\right), \tag{53}$$

with the same scaling variable $\tilde{\eta}$ as in the preceding section. Similarly, using (A11) gives

$$\mathcal{Z}_{\|}(\zeta) \approx \frac{1}{1.49}\sum_{k=0}^{\infty}(-1)^k\sum_{i=4}^{8}\lambda_{2k+i/4}^{-1}e^{-\lambda_{2k+i/4}^2\tilde{\eta}}. \tag{54}$$

Hence, as in 3D, one finds for the free energy

$$\mathcal{F}_{\|}(\zeta,L,\ell_p) = -k_BT\ln\tilde{\mathcal{Z}}_{\|}(\tilde{\eta}) \tag{55}$$

and the entropic force

$$f_{\|}(\zeta,L,\ell_p) = f_c\tilde{f}_{\|}(\tilde{\eta}) \tag{56}$$

with the scaling function

$$\tilde{f}_{\|}(\tilde{\eta}) = -\frac{4}{\pi^2}\frac{\tilde{\mathcal{Z}}_{\|}'(\tilde{\eta})}{\tilde{\mathcal{Z}}_{\|}(\tilde{\eta})}, \tag{57}$$

where $f_c = \pi^2\kappa/4L^2$; see the solid curves in Fig. 6 and Fig. 7 for a plot of the scaling functions for the free energy and entropic force, respectively. The key difference between the results in 2D and 3D is that the effective free energy exhibits a change in curvature at $\tilde{\eta} \approx 0.05$ and as a result a pronounced peak in the entropic force. The peak is a pretty robust feature of the distribution function and vanishes only for very large values of $\varepsilon \approx 5$.

In order to understand the physical origin of this peak it suffices to consider small values of $\tilde{\eta}$. Then, using only the leading term of the series expansion (53), one obtains for the entropic force

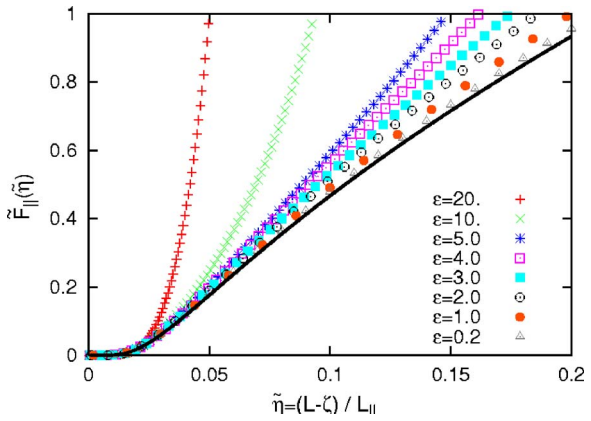

FIG. 6. (Color online) Free energy of a grafted polymer whose tip is constrained by a rigid wall in 2D. The solid line gives the universal scaling function in the stiff limit. MC data are given by the symbols for different values of the stiffness parameter ε as indicated in the graph.

$$\tilde{f}_{\|}^{<}(\tilde{\eta}) = \frac{\sqrt{2}e^{-1/16\tilde{\eta}}}{\pi^{5/2}\tilde{\eta}^{3/2}[1-\sqrt{2}\,\mathrm{erfc}(1/4\sqrt{\tilde{\eta}})]}. \tag{58}$$

This has the same functional form as the corresponding expression in 3D, (45), but differs in some numerical factors. These differences can all be traced back to the strength α of the essential singularity of the tip distribution function close to full stretching, $\tilde{P}_{\|}(\tilde{\rho}) \propto \exp(-\alpha/\tilde{\rho})$; compare (35) with (51). One may interpret this strength as a kind of phase space factor counting how fast the number of polymer configurations decreases as one approaches full stretching. It clearly shows that the maximum of the entropic force in 2D is of purely geometric origin. As an interesting consequence of this maximum, one should note that for most values of the reduced stored length $\tilde{\eta}$ the entropic force *exceeds* the purely mechanical force given by the Euler buckling force.

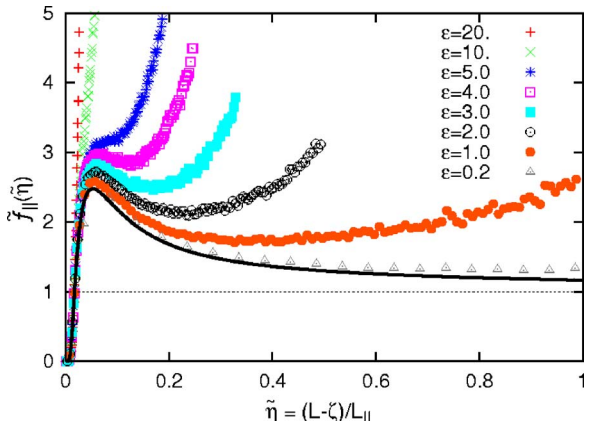

FIG. 7. (Color online) Scaling function for the entropic force which a grafted polymer exerts on a rigid wall in 2D as a function of the reduced stored length $\tilde{\eta}=(L-\zeta)/L_{\|}$. The solid line gives the universal scaling function in the stiff limit. MC data are given by the symbols for different values of the stiffness parameter ε as indicated in the graph. There is a pronounced peak in the entropic force for $\varepsilon < 5$.

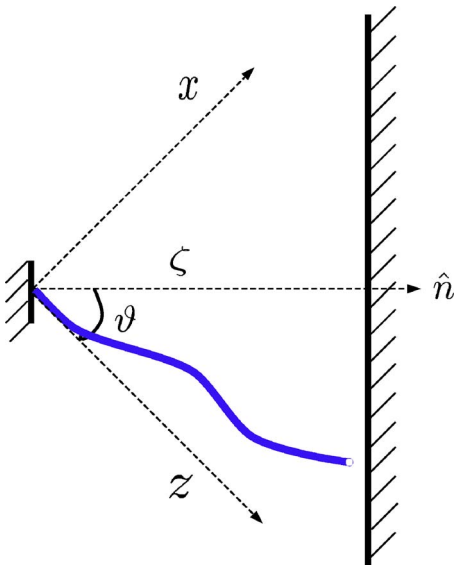

FIG. 8. (Color online) A smooth hard wall at some oblique angle $\pi/2-\vartheta$, constrains the configurations of a stiff polymer grafted parallel to the z axis.

IV. GRAFTED POLYMER AT AN OBLIQUE ANGLE TO THE WALL

The generic situation one encounters in a cellular system is that the polymer is inclined with respect to a membrane. Then we must ask how the force derived above changes when the graft of the polymer is not orthogonal to the constraining wall but at some oblique angle $\pi/2-\vartheta$; see Fig. 8. Since the presence of the wall restricts the position of the polymer tip to

$$r_z(L)\cos\vartheta + r_x(L)\sin\vartheta \leqslant \zeta \tag{59}$$

one must evaluate the restricted partition sum,

$$\mathcal{Z}(\zeta,\vartheta) = \langle \Theta(\zeta - r_z(L)\cos\vartheta - r_x(L)\sin\vartheta)\rangle_0$$
$$= \int dxdz P(x,z)\Theta(\zeta - z\cos\vartheta - x\sin\vartheta) \tag{60}$$

to find the entropic force.

A. Probability distribution function of the tip

This calculation requires the knowledge of the joint probability density of the tip

$$P(x,z) := \langle \delta(r_x(L)-x)\,\delta(r_z(L)-z)\rangle_0. \tag{61}$$

In Sec. III, we have already analyzed the reduced distribution function $P_{\|}(z)$ and found that its width is characterized by the scale $L_{\|}=L^2/\ell_p$. Similarly, one can find an explicit expression for $P_{\perp}(x)$ in harmonic approximation, where

$$r_x(L) \approx \sum_{k=1}^{\infty} a_{x,k}\int_0^L ds\,\sin(\lambda_k s/L) = L\sum_{k=1}^{\infty}\lambda_k^{-1}a_{x,k}, \tag{62}$$

and thus

$$P_\perp(x) = \int \frac{dq}{2\pi} e^{iqx} \left\langle \exp\left(- iqL \sum_{k=1}^{\infty} \lambda_k^{-1} a_{x,k} \right) \right\rangle$$
$$= \int \frac{dq}{2\pi} e^{iqx} \exp\left(- \frac{L^3}{\ell_p} q^2 \sum_{k=1}^{\infty} \lambda_k^{-4} \right). \quad (63)$$

With $\Sigma_{k=1}^{\infty} \frac{1}{(2k-1)^4} = \frac{\pi^4}{96}$ [21], this gives a Gaussian distribution

$$P_\perp(x) = \frac{1}{\sqrt{2\pi} L_\perp} e^{-(1/2)(x/L_\perp)^2}, \quad (64)$$

where we have defined the characteristic *transverse length scale*

$$L_\perp = \sqrt{L^3/3\ell_p}. \quad (65)$$

Together with $L_\parallel$, these are the two length scales are characterizing the width of the joint distribution function. This suggests to write the joint distribution function as

$$P(x,z,L,\ell_p) = \frac{1}{L_\parallel L_\perp} \tilde{P}(\tilde{x},\tilde{\rho}), \quad (66)$$

in terms of dimensionless variables

$$\tilde{x} = x/L_\perp, \quad (67)$$

$$\tilde{\rho} = (L-z)/L_\parallel. \quad (68)$$

An explicit form of the joint distribution function can be calculated to harmonic order. For simplicity, we start with a polymer fluctuating only in the x-z plane ($d=2$). Then

$$P_2(x,z) = \int \frac{dq_z}{2\pi} \frac{dq_x}{2\pi} e^{-iq_z z - iq_x x} \langle e^{i[q_z r_z(L) + q_x r_x(L)]} \rangle_0$$
$$= \int \frac{dq_z}{2\pi} \frac{dq_x}{2\pi} e^{iq_z(L-z) - iq_x x} \prod_k \left\langle \exp\left[- i\left(\frac{Lq_z}{4} a_{x,k}^2 - \frac{Lq_x}{\lambda_k} a_{x,k} \right) \right] \right\rangle$$
$$= \int \frac{dq_z}{2\pi} \frac{dq_x}{2\pi} e^{iq_z(L-z) - iq_x x} \prod_k \sqrt{\frac{\lambda_k^2}{\lambda_k^2 + iq_z L_\parallel}} \exp\left(- \frac{3q_x^2 L_\perp^2}{\lambda_k^2(\lambda_k^2 + iq_z L_\parallel)} \right)$$
$$= \frac{1}{L_\perp L_\parallel} \int \frac{d\tilde{q}_z}{2\pi} \frac{d\tilde{q}_x}{2\pi} e^{i\tilde{q}_z\tilde{\rho} - i\tilde{q}_x\tilde{x}} \left(\prod_k \sqrt{\frac{1}{1 + i\tilde{q}_z \lambda_k^{-2}}} \right) \exp\left(- 3\tilde{q}_x^2 \sum_k \frac{1}{\lambda_k^2(\lambda_k^2 + i\tilde{q}_z)} \right)$$
$$= \frac{1}{L_\perp L_\parallel} \int \frac{d\tilde{q}_z}{2\pi} \frac{d\tilde{q}_x}{2\pi} a_2(i\tilde{q}_z) e^{i\tilde{q}_z\tilde{\rho} - i\tilde{q}_x\tilde{x}} \exp\left(- \frac{3}{2} \tilde{q}_x^2 b(i\tilde{q}_z) \right), \quad (69)$$

where for $z \in \mathbb{R}_+$ we have [21]

$$a_2(z) := \prod_k \sqrt{\frac{1}{1 + z\lambda_k^{-2}}} = \sqrt{\frac{1}{\cosh\sqrt{z}}}, \quad (70)$$

$$b(z) := 2 \sum_k \frac{1}{\lambda_k^2(\lambda_k^2 + z)} = \frac{\sqrt{z} - \tanh\sqrt{z}}{z^{3/2}}. \quad (71)$$

For $d=3$, the additional degrees of freedom associated with excursions in the y direction lead to the replacement of $q_z a_x^2(k)$ by $q_z[a_x^2(k) + a_y^2(k)]$ which results in an additional factor of $\sqrt{1 + iq_z\lambda_k^{-2}}$ for each mode k. Thus, for general d, we have to replace $a_2(z)$ with

$$a_d(z) := \prod_k \left(\frac{1}{1 + z\lambda_k^{-2}} \right)^{(d-1)/2}. \quad (72)$$

As $\mathrm{Re}[b(i\tilde{q}_z)] > 0$ for all $\tilde{q}_z \in [-\infty, \infty]$, the Gaussian integration over $\tilde{q}_x$ in Eq. (69) can be performed by completing the square, such that

$$\tilde{P}_d(\tilde{x},\tilde{\rho}) = \int \frac{d\tilde{q}_z}{2\pi} e^{i\tilde{q}_z\tilde{\rho}} \frac{a_d(i\tilde{q}_z)}{\sqrt{6\pi b(i\tilde{q}_z)}} \exp\left(- \frac{\tilde{x}^2}{6b(i\tilde{q}_z)} \right). \quad (73)$$

Along similar lines, one may also calculate the full joint distribution function for a grafted polymer in $d=3$,

$$P_3(x,y,z) = \frac{1}{L_\perp^2 L_\parallel} \int \frac{d\tilde{q}_z}{2\pi} e^{i\tilde{q}_z\tilde{\rho}} \frac{a_3(i\tilde{q}_z)}{6\pi b(i\tilde{q}_z)} \exp\left(- \frac{\tilde{x}^2 + \tilde{y}^2}{6b(i\tilde{q}_z)} \right)$$
$$=: \frac{1}{L_\perp^2 L_\parallel} \tilde{P}_3(\tilde{x},\tilde{y},\tilde{\rho}). \quad (74)$$

In addition to the poles of $a_3(i\tilde{q}_z)$ at $\tilde{q}_z = i\lambda_k^2$ on the positive imaginary axis of the $\tilde{q}_z$ plane, the integrand also has singularities at the zeros $i\lambda_k^2$ of $b(z)$. Thus we continue by evaluating the integrals numerically.

1. Numerical evaluation of integrals

The integrand of (73) has no singularities on the real $\tilde{q}_z$ axis. Before attempting a numerical integration, we discuss the behavior of the different terms appearing in (73). For $d=3$, we have

$$a_3(z) = \prod_k \frac{1}{1 + z\lambda_k^{-2}} = \frac{1}{\cosh\sqrt{z}}. \tag{75}$$

For $\tilde{q}_z \in \mathbb{R}$, the real and the imaginary part $1/\cosh\sqrt{i\tilde{q}_z}$ are, respectively, even and odd functions rapidly decaying in magnitude for $\tilde{q}_z \to \pm\infty$. The real part of $1/b(i\tilde{q}_z)$ is strictly positive and increasing with increasing $|\tilde{q}_z|$. The imaginary part of $1/b(i\tilde{q}_z)$ behaves asymptotically as $\mathrm{Im}[b^{-1}(i\tilde{q}_z)] \sim \tilde{q}_z$ leading to a second strongly oscillating contribution to the integrand of (73) besides $\exp(iqz)$. In the interest of numerical stability of the integration, it is advantageous to rewrite the integrand appearing in (73) to

$$\frac{1}{2\pi} e^{iq(\tilde{\rho}-\tilde{x}^2/6)} \frac{a_3(iq)}{\sqrt{2\pi 3 b(iq)}} \exp\left(-\frac{\tilde{x}^2}{6}[1/b(iq) - iq]\right) \tag{76}$$

for q larger than some fixed q_0.

2. Region of vanishing probability

Equation (76) suggests that $\tilde{\rho}=\tilde{x}^2/6$ is a special situation. The probability density $P(x,z)$ must vanish for points which are at distances greater than L from the graft, $x^2+z^2 \leqslant L^2$. What does this translate to in the harmonic approximation? The largest value x^* of $r_x(L)$ that can be obtained for a given value z^* of $r_z(L)$ can be found from the variation of $r_x(L) - \rho[z^* - r_z(L)]$ where ρ is a Lagrange multiplier. Using (18) and (62), this leads to $a_{x,k}=a/\lambda_k$ where a is some number. We thus find

$$x^* = La\sum_{k=1}^{\infty} \lambda_k^{-2} = L\frac{a}{2} \tag{77}$$

and

$$z^* = L - \frac{L}{4}a^2\sum_{k=1}^{\infty} \lambda_k^{-2} = L - L\frac{a^2}{8} \tag{78}$$

resulting in

$$\frac{L - z^*}{L} = \frac{1}{2}\left(\frac{x^*}{L}\right)^2. \tag{79}$$

As $L_\perp^2/LL_\parallel = 1/3$, this is equivalent to

$$\tilde{\rho}^* = \tfrac{1}{6}(\tilde{x}^*)^2. \tag{80}$$

Hence $\tilde{P}(\tilde{x},\tilde{\rho})$ must vanish for $\tilde{\rho} < \tilde{x}^2/6$.

3. Results for the general distribution function

It is now straightforward to evaluate the integrals in Eq. (73) by some standard numerical method. The corresponding results are shown in Fig. 9 as contour plots of $\tilde{P}(\tilde{x},\tilde{\rho})$ in $d=3$ and $d=2$, respectively. These analytical results compare very well with MC results for polymers with a stiffness parameter $\varepsilon \leqslant 0.2$; see a plot with $\varepsilon=0.1$ in Fig. 10. There are deviations between the harmonic approximation and MC data for larger values of ε [19,20,25].

The density distribution essentially vanishes outside the parabola given by $\tilde{\rho}=\tilde{x}^2/6$, corresponding to the classical contour of the polymer in harmonic order. The main weight of $\tilde{P}(\tilde{x},\tilde{\rho})$ is concentrated close to this line, where the effect is stronger for $d=2$. Profiles parallel to the $\tilde{\rho}$ direction are of a shape qualitatively similar to $\tilde{P}_\parallel(\tilde{\rho})$ (see Fig. 2) at least for small $\tilde{x}$. Profiles parallel to the $\tilde{x}$ axis are not Gaussian. For small $\tilde{\rho} \lessapprox 0.1$, they are peaked at $\tilde{x}=0$ but unlike a Gaussian,

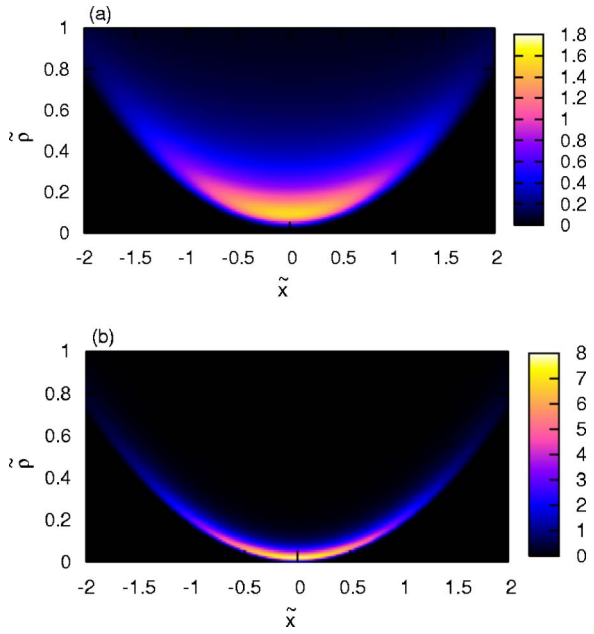

FIG. 9. (Color online) Density plot of the probability density $\tilde{P}(\tilde{x},\tilde{\rho})$ in (a) $d=3$ and (b) $d=2$ calculated numerically from Eq. (73). As it is expected, the probability distribution of the tip is much narrower in 2D compare to 3D.

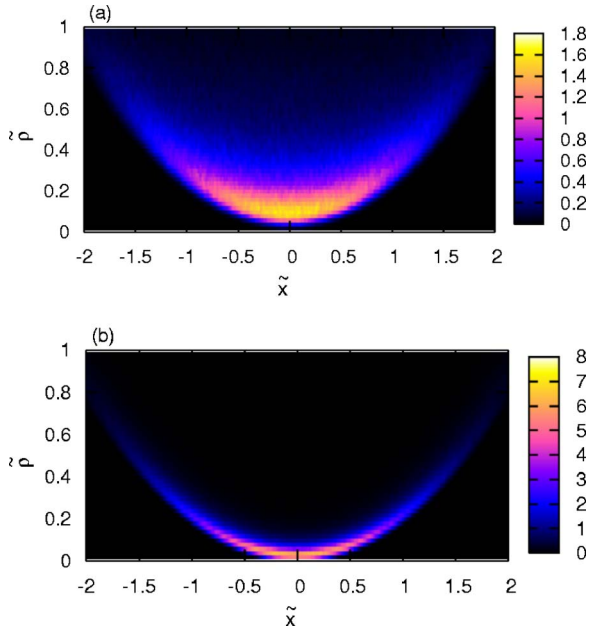

FIG. 10. (Color online) Density plot of the probability density $\tilde{P}(\tilde{x},\tilde{\rho})$ in (a) $d=3$ and (b) $d=2$ obtained from MC simulations for $\varepsilon=0.1$. The MC data agree very well with corresponding numerical results in Fig. 9.

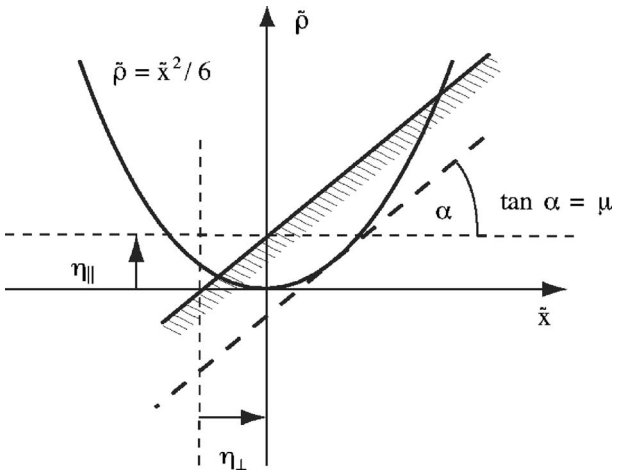

FIG. 11. Geometry of the problem in terms of the reduced coordinates $\tilde{x}$ and $\tilde{\rho}$. The position of the wall is characterized by its slope $\mu=\eta_\parallel/\eta_\perp$ and $\eta_\parallel$, the distance from the origin along the $\tilde{z}$ axis, i.e., the minimal reduced stored length imposed by the presence of the constraining wall. To harmonic order the finite length of the filament also constrains the reduced stored length $\tilde{\rho}$ to be larger than $\tilde{x}^2/6$.

they vanish for $\tilde{x}^2>6\tilde{\rho}$. For larger $\tilde{\rho}$, they display a double-peaked shape. Both features would be completely missed by a factorization approximation $\tilde{P}(\tilde{x},\tilde{\rho})=\tilde{P}_\perp(\tilde{x})\tilde{P}_\parallel(\tilde{\rho})$. An elaborate discussion of the features of the distribution function in $d=2$ and $d=3$, as one increases the stiffness parameters or introduces some backbone elasticity, will be the topic of a forthcoming presentation [25].

The shape of the full joint probability distribution $P_3(x,y,z)$ is best illustrated by plotting an isosurface, e.g., $\tilde{P}_3(\tilde{x},\tilde{y},\tilde{\rho})=0.1$. Due to rotational symmetry, a density plot for $P_3(x,y,z)$ may be obtained by rotating the contour plot of $P_3(x,z)$ [Fig. 9(a)] around the z axis. Again MC and analytical results are identical for small ε.

B. Entropic forces: scaling functions

We are now in a position to evaluate the general expression (60), for the restricted partition sum. Before going into the details of the calculations, it is instructive to have a look at the geometry of the problem in terms of the dimensionless variables $\tilde{x}$ and $\tilde{\rho}$. Recall that $\tilde{x}$ and $\tilde{\rho}$ are measuring the transverse displacement of the tip x and the stored length $L-z$ in units of the characteristic transverse and longitudinal length scales, $L_\perp$ and $L_\parallel$, respectively. As can be inferred from Fig. 8, the wall crosses the $\tilde{x}$ and $\tilde{\rho}$ axis at

$$\eta_\perp = \frac{L\cos\vartheta-\zeta}{L_\perp\sin\vartheta} \quad \text{and} \quad \eta_\parallel = \frac{L\cos\vartheta-\zeta}{L_\parallel\cos\vartheta}, \tag{81}$$

respectively; see Fig. 11. These are the two basic dimensionless variables characterizing the entropic forces exerted on the inclined wall. We also introduce the slope $\mu=\tan\alpha$ of the constraining wall with respect to the $\tilde{x}$ axis

$$\mu = \frac{\eta_\parallel}{\eta_\perp} = \frac{L_\perp}{L_\parallel}\tan\vartheta = \frac{1}{\sqrt{3\varepsilon}}\tan\vartheta. \tag{82}$$

As discussed above, the finite length of the polymer gives a constraint on the reduced stored length $\tilde{\rho}$ such that it must be larger than $\tilde{x}^2/6$, i.e., above the parabola drawn in Fig. 11. Hence, just the points on the constraining wall inside the parabola are accessible to the tip of the polymer. As one moves the wall further away from the grafted end, the number of contact points decreases and finally reduces to zero when the wall becomes tangent to the parabola. In this limit, where

$$\eta_\parallel^c = -\tfrac{3}{2}\mu^2 \tag{83}$$

the force exerted on the wall vanishes.

We may now write the restricted partition sum in terms of the reduced stored length $\eta_\parallel$ and the slope of the wall μ,

$$\mathcal{Z}(\zeta,\vartheta) = \tilde{\mathcal{Z}}(\eta_\parallel,\mu), \tag{84}$$

where

$$\tilde{\mathcal{Z}}(\eta_\parallel,\mu) = \frac{1}{2}\,\mathrm{erfc}\,\frac{\eta_\parallel}{\sqrt{2}\mu} - \int_0^\infty \frac{dq}{\pi q} \times \mathrm{Im}[e^{iq\eta_\parallel}(a_3(iq)e^{-(3/2)(\mu q)^2 b(iq)} - e^{-(1/2)(\mu q)^2})], \tag{85}$$

as shown in Appendix D. The force is again found by taking the derivative of $k_BT\ln\mathcal{Z}$ with respect to ζ. It obeys the scaling law

$$f(\zeta,\vartheta,L,\ell_p) = f_c(\vartheta)\tilde{f}(\eta_\parallel,\mu), \tag{86}$$

with an amplitude

$$f_c(\vartheta) = \frac{\pi^2\kappa}{4L^2\cos\vartheta} = \frac{f_c}{\cos\vartheta} \tag{87}$$

and a scaling function

$$\tilde{f}(\eta_\parallel,\mu) = -\frac{4}{\pi^2}\frac{\tilde{\mathcal{Z}}'(\eta_\parallel,\mu)}{\tilde{\mathcal{Z}}(\eta_\parallel,\mu)} \tag{88}$$

that can be expressed in terms of the restricted partition sum and its derivative

$$\tilde{\mathcal{Z}}'(\eta_\parallel,\mu) = -\int_0^\infty \frac{dq}{\pi}\,\mathrm{Re}(e^{iq\eta_\parallel}a_3(iq)e^{-(3/2)(\mu q)^2 b(iq)}). \tag{89}$$

As detailed in Appendix D, Eq. (85) and Eq. (89) are suited best for a numerical evaluation of the entropic force.

In Fig. 12, the analytical results for the scaling function $\tilde{f}(\eta_\parallel,\mu)$ of the entropic force are shown as a function of $\delta\eta_\parallel=\eta_\parallel-\eta_\parallel^c$, for a series of values of μ. Since we have subtracted off the critical value of the reduced stored length $\eta_\parallel^c$, the forces vanish for $\delta\eta_\parallel\leqslant 0$. There is a dramatic difference in the shape of the force-distance curves in 2D and 3D. Whereas the force increases monotonically with increasing $\delta\eta_\parallel$ for 3D, it shows a pronounced maximum in 2D, the

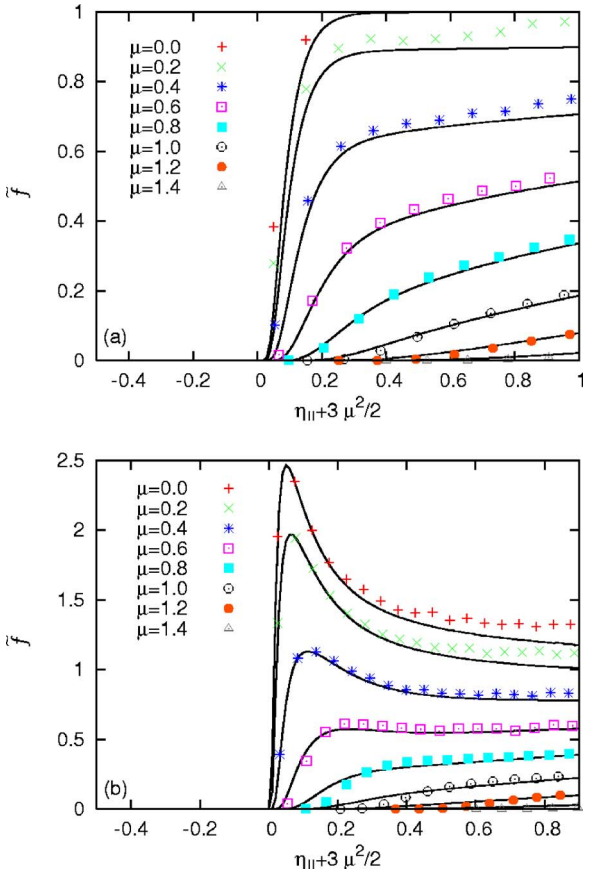

FIG. 12. (Color online) Scaling function of the entropic force $\tilde{f}$ in (a) $d=3$ and (b) $d=2$ as a function of $\delta\eta_{\|}=\eta_{\|}+\frac{3}{2}\mu^2$ for a series of values of μ as indicated in the graphs. Solid lines represent analytical results as obtained from a numerical evaluation of Eq. (88). Monte Carlo data for a stiffness parameter $\varepsilon=0.1$ are given as symbols, as indicated in the graphs. For $\mu=0$, one recovers the results for $\tilde{f}_{\|}(\eta_{\|})$ as discussed in Sec. III.

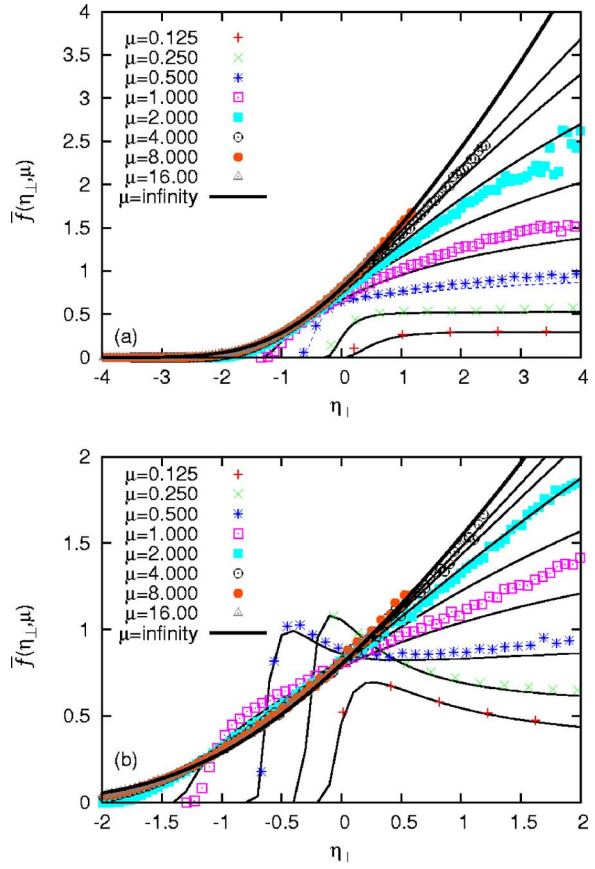

FIG. 13. (Color online) Scaling function $\bar{f}(\eta_{\perp},\mu)$ in (a) $d=3$ and (b) $d=2$ for a series of values for μ (solid lines). For large μ, the scaling function $\bar{f}(\eta_{\perp},\mu)$ asymptotically converges to $\bar{f}_{\perp}(\eta_{\perp})$ obtained within a factorization approximation. The MC data indicated by different symbols in the graphs are given for a fixed stiffness parameter $\varepsilon=0.1$.

physical origin of which is the same as for $\vartheta=0$. The maximum in 2D vanishes upon increasing μ, which can either be understood as an increase in the inclination angle or an increase in the persistence length; see Eq. (82).

For comparison, MC data are given for a particular value of the stiffness parameter, $\varepsilon=0.1$. In this stiff regime the analytical results compare very well with the MC data, except for large values in the stored length where the harmonic approximation is expected to become invalid.

For small values of μ, the reduced stored length $\eta_{\|}$ is no longer a good variable. Instead, we define a new scaling function $\bar{f}(\eta_{\perp},\mu)$ such that

$$f(\zeta,\vartheta)=\frac{k_BT}{L_{\perp}\sin\vartheta}\bar{f}(\eta_{\perp},\mu), \tag{90}$$

where

$$\bar{f}(\eta_{\perp},\mu)=\mu\frac{\pi^2}{4}\tilde{f}(\eta_{\|}/\mu,\mu). \tag{91}$$

Like in the previous scaling plot, the force should vanish for $\delta\eta_{\|}<0$, which in terms of $\eta_{\perp}$ reads $\eta_{\perp}<-\frac{3}{2}\mu$. Again, there is a marked difference between 2D and 3D results; see Fig. 13. We also observe that the scaling function $\bar{f}(\eta_{\perp},\mu)$ asymptotically approaches a limiting curve for $\mu\to\infty$, which for a fixed value of ε, corresponds to $\vartheta\to\pi/2$. It turns out, as we will show now, that this limiting behavior can well be explained within a factorization approximation $P(x,z)\approx P_{\|}(z)P_{\perp}(x)$. Then, $\mathcal{Z}(\zeta,\vartheta)$ simplifies to

$$\mathcal{Z}(\zeta,\vartheta)=\int dz P_{\|}(z)\mathcal{Z}_{\perp}(\zeta\sin^{-1}\vartheta-z\cot\vartheta), \tag{92}$$

where

$$\mathcal{Z}_{\perp}(x)=\int_{-\infty}^{x}dx'P_{\perp}(x') \tag{93}$$

is the restricted partition sum for the transverse fluctuations. The longitudinal distribution function $P_{\|}(z)$ is, for small L/ℓ_p, strongly peaked at $z\approx L$ with a characteristic width of $L_{\|}$, and $\mathcal{Z}_{\perp}$ varies on the scale $L_{\perp}$. Then, for $\mu\gg1$, the width of the longitudinal distribution function is much smaller than

the transverse restricted partition sum, such that the integration over $P_\parallel$ can be approximated by $\mathcal{Z}(\zeta,\vartheta)\approx\mathcal{Z}_\perp[(\zeta - L\cos\vartheta)\sin^{-1}\vartheta]$ which upon using that the transverse distribution function is a simple Gaussian, Eq. (64), results in

$$\mathcal{Z}(\zeta,\vartheta)\approx\frac{1}{2}\,\mathrm{erfc}\,\frac{\eta_\perp}{\sqrt{2}}=:\bar{\mathcal{Z}}_\perp(\eta_\perp). \tag{94}$$

This approximation fails when $\mu\approx 1$, which defines an angle

$$\vartheta_c=\arctan(L_\parallel/L_\perp)\approx\sqrt{3L/\ell_p} \tag{95}$$

well above which the factorization approximation is valid. The entropic force is then

$$f(\zeta,\vartheta)=\frac{k_BT}{L_\perp\sin\vartheta}\bar{f}_\perp(\eta_\perp), \tag{96}$$

where

$$\bar{f}_\perp(\eta_\perp)=-\frac{\bar{\mathcal{Z}}'_\perp(\eta_\perp)}{\bar{\mathcal{Z}}_\perp(\eta_\perp)}=\sqrt{\frac{2}{\pi}}\frac{e^{-\eta_\perp^2/2}}{\mathrm{erfc}(\eta_\perp/\sqrt{2})}. \tag{97}$$

This result for the scaling function of the entropic force is indicated as the thick solid line in Fig. 13. It becomes exact in the limit $\vartheta=\pi/2$, where starting from Eq. (60) one can integrate out the longitudinal coordinate to end up with

$$\mathcal{Z}\left(\zeta,\frac{\pi}{2}\right)=\frac{1}{2}\,\mathrm{erfc}\left(\frac{-\zeta}{\sqrt{2}L_\perp}\right). \tag{98}$$

Finally, for large ζ, one recovers the linear response result $f(\zeta,\pi/2)=3\kappa\zeta/L^3$.

If we compare the results of the factorization approximation for $\vartheta>\vartheta_c$, (96) and (97), to Eq. (2) and Eq. (5) of Ref. [7], one realizes that they are almost identical up to the minor difference that Mogilner and Oster define their κ_0 to be $4\kappa/L^3$ where it actually should be $3\kappa/L^3$. The factor 4 in Ref. [7] instead of the correct value 3 is the result of assuming that the minimal energy configuration of a thin rod bent by application of a force to its nongrafted end has constant radius of curvature for small deflections, which is not the case. In fact, the boundary condition of the mechanical problem forces the curvature to vanish at the nongrafted end. In Ref. [7], the entropic force was calculated by taking into account the transverse fluctuations of the grafted polymer only and completely disregarding any stored length fluctuations. Here, the factorization approximation, which treats longitudinal and transverse fluctuations as independent, gives the same result for inclination angles $\vartheta>\vartheta_c$. The reason behind the validity of the asymptotic results, (96) and (97), is that the tip distribution function is much narrower in the longitudinal than the transverse direction for $\vartheta\gg\vartheta_c\sim\sqrt{L/\ell_p}$. Hence the range of validity of the factorization approximation becomes larger as the polymers become stiffer. Of course, the analysis in Ref. [7] has to fail for small inclination angles since it does not account for stored length fluctuations at all. This is seen most dramatically for $\vartheta=0$, where such an approximation would give no force at all in contrast to what we find in Sec. III.

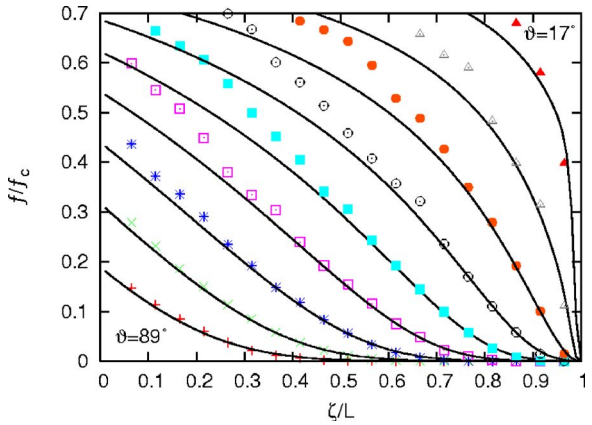

FIG. 14. (Color online) Analytical and MC simulation results for the entropic force f/f_c as a function of the distance of the grafted end from the wall ζ/L for a series of inclination angles $\vartheta=17°,\ldots,89°$ with steps 9° ($d=3$).

C. Entropic forces: explicit results

The analysis in the preceding section gives the full scaling picture for the entropic forces as a function of the scaling variables $\eta_\parallel$ and $\eta_\perp$. Here we discuss our findings in terms of the actual distance of the grafted end to the wall ζ, the inclination angle ϑ, and the stiffness parameter $\varepsilon=L/\ell_p$, which may be more convenient for actual applications. Of course, the disadvantage of such a representation is that we now must give the results for particular values of the stiffness parameter. In this section, we first discuss the results in 3D and then compare it to the 2D case.

In Figs. 14 and 15, the force f in units of the Euler buckling force f_c is shown as a function of ζ (in units of the total filament length L) for a series of values of ϑ and vice versa ($d=3$); the stiffness parameter has been taken as $\varepsilon=0.1$. Recall that the angle $\vartheta=0$ corresponds to a wall perpendicular to the orientation of the grafted end of the polymer, which has been discussed in detail in Sec. III. Upon increasing the inclination angle ϑ, the entropic force decreases for all given values of ζ. This is to be expected since the wall then cuts off

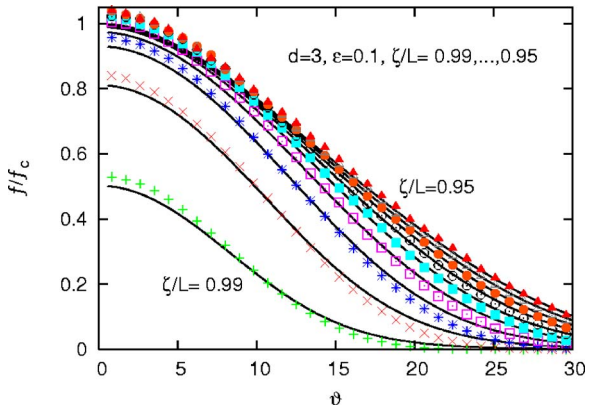

FIG. 15. (Color online) Analytical and MC simulation results for the entropic force f/f_c as a function of the inclination angle ϑ (in degrees) for a series of distances to the wall $\zeta/L=0.99,0.985,\ldots,0.95$.

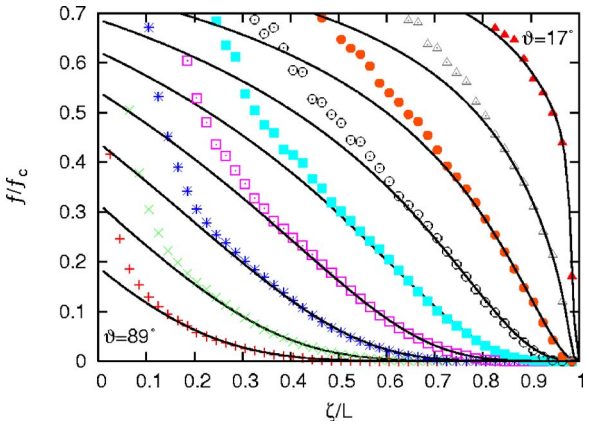

FIG. 16. (Color online) Comparison of the analytical results for the entropic force as a function of ζ/L (solid lines) for a series of values for $\vartheta=17°,\ldots,89°$ with steps 9° indicated in the graph with MC simulations (symbols in the graph), which take into account the constraints of the wall on the body of the polymer; $\varepsilon=0.1$. The deviations are most pronounced for small values of ζ and inclination angles ϑ close to $\pi/2$ ($d=3$).

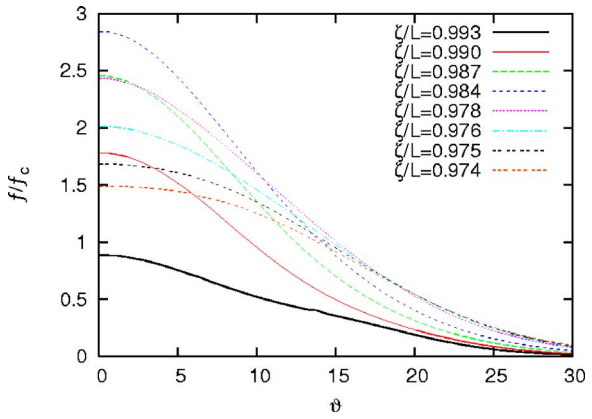

FIG. 17. (Color online) Analytical results for the entropic force f/f_c as a function of the inclination angle ϑ (in degrees) for different values of distances to the wall ($d=2$); stiffness parameter has been taken as $\epsilon=0.1$. MC data points have been removed for more clarity.

less from the probability cloud of the polymer tip. For the same reason the forces also decrease with increasing ζ for a given value of ϑ. The analytical results (solid lines) agree well with the MC data for not too small values of ζ. The deviations grow larger upon decreasing the distance between the wall and the grafted end. Then nonlinear effects are not taken into account by our weakly bending approximation set.

In the limit as the inclination angle approaches $\pi/2$, it is certainly no longer justified to calculate the entropic force by assuming that only the polymer tip is not allowed to penetrate the membrane. Then, one must take into account the fact that also the body of the polymer is constrained by the presence of the wall. Since this reduces the number of allowed polymer configurations even further, this effect is expected to lead to an enhancement of the entropic force. Indeed this is the case, as one may infer from Fig. 16, where we show a comparison with MC simulation accounting for these constraints. One also notes that the enhancement of the entropic forces becomes largest as $\vartheta\to\pi/2$ and the distance between the wall and the grafted end becomes small; a full account of this effect will appear in Ref. [26].

For comparison, Fig. 17 shows the entropic force f in 2D as a function of ϑ for different values of ζ. Inspection of this figure immediately tells us that in contrast to 3D decreasing ζ (for a given value of ϑ) is not always increasing the entropic force.

Finally, we would like to compare our full results in 3D with the factorization approximation discussed in the preceding section, Eq. (97), which when corrected for some minor factor is identical to the results given in Ref. [7]. The comparison is given in Fig. 18 for a stiffness parameter $\varepsilon=0.1$. In the limit of large inclination angles well above $\vartheta_c\approx 30°$, there is excellent agreement between the factorization approximation and the full results for not too small values of ζ. As one approaches ϑ_c, the range of validity of the factorization approximation shrinks and finally it becomes invalid for $\vartheta<\vartheta_c$.

To illustrate the applicability of the factorization approximation, let us take some examples. For the cytoskeletal filament F-actin with a contour length 100 nm and persistence length $\ell_p=15\ \mu$m, the stiffness parameter becomes $\varepsilon=0.006$ which gives $\vartheta_c\approx 7.6°$. Upon increasing the stiffness parameter to $\varepsilon=0.1$, which amounts to changing the contour length to a value of $L=1.6\ \mu$m, the critical angle ϑ_c increases to 28.7°.

V. PROTRUSION VELOCITY AND INTERCALATION PROBABILITY

In this final section, we would like to apply our results to calculate the protrusion velocity for an idealized model system. This serves to illustrate how the theoretical results obtained in this paper may be applied to arrive at a microscopic

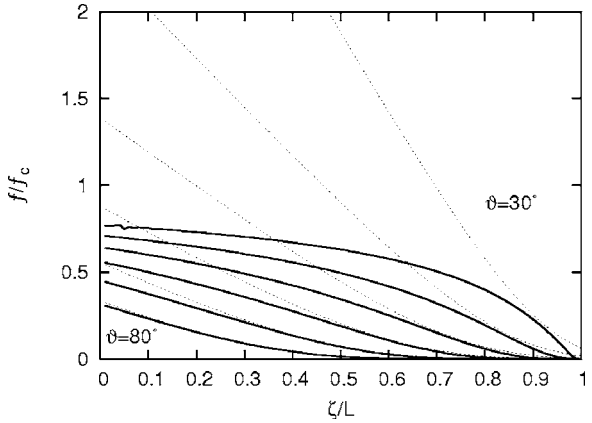

FIG. 18. Comparison of the full result for the entropic force as a function of ζ/L (full lines) with the results obtained from the factorization approximation (dashed lines) for a stiffness parameter $\varepsilon=0.1$ and a series of inclination angles $\vartheta=30°,40°,\ldots,80°$. The range of validity of the factorization approximation broadens as one increases the inclination angle ϑ; it is invalid for ϑ smaller than $\vartheta_c\approx 30°$.

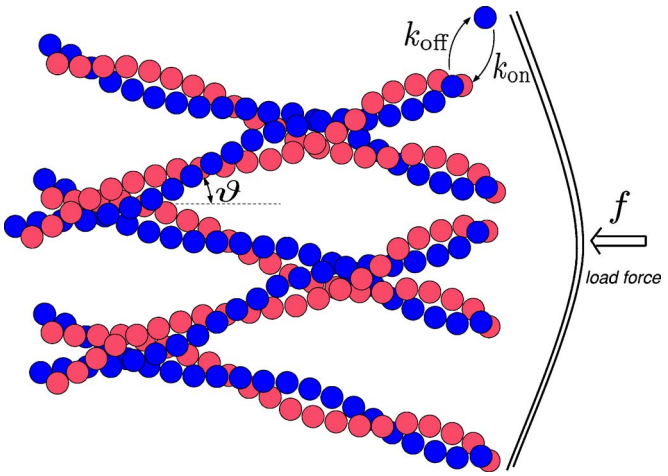

FIG. 19. (Color online) An actin network polymerizing in the presence of an external load. ϑ is the network orientation, k_{on} is the monomers attachment rate, and k_{off} is the monomers detachment rate. The membrane—for simplicity—has been idealized as a rigid smooth wall.

model for cell motility. As illustrated in Fig. 19, we consider a semiflexible polymer mesh, where each filament is inclined at a fixed angle ϑ with respect to a membrane, which—for simplicity—is idealized as a rigid smooth wall. We ask for the average protrusion velocity of the polymerizing mesh pushing against a membrane which is under a constant external load f.

For a monomer to be appended to the tip of fluctuating semiflexible polymer near the rigid wall, the distance between tip and the wall must be at least $\delta \cos \vartheta$ where δ is the increase in polymer length due to the addition of a single monomer. For actin, δ would be half a monomer radius or $\delta \approx 2.7$ nm. The intercalation probability is given by

$$p(\zeta, \vartheta, \delta) = \frac{Z(\zeta - \delta \cos \vartheta, \vartheta)}{Z(\zeta, \vartheta)}. \tag{99}$$

Biologically relevant parameters are $L \approx 30$ nm and $l_p \approx 15$ μm which corresponds to $\vartheta_c = 4.5°$ and a critical force of $f_c \approx 150$ pN. For a given external force f, we may now find ζ and ϑ such that $f(\zeta, \vartheta) = f$. Then, following Ref. [7], the intercalation probability can (under certain assumptions) be converted into a protrusion velocity of the tip

$$v(f, \vartheta) = \delta \cos \vartheta (k_{on} M p[\zeta(f, \vartheta), \vartheta, \delta] - k_{off}), \tag{100}$$

where M is the monomer concentration and k_{on} and k_{off} are the monomers attachment and detachment rates, respectively. Figure 20 displays the velocity as a function of the inclination angle ϑ and a set of forces ranging from 0.1 pN to 2.9 pN. The main feature of this figure is that the filament growth velocity is not a monotonic function of the angle ϑ, but passes through a maximum at an optimal filament orientation ϑ_{opt}. The physical reason for such an optimal angle is obvious. On the one hand, thermal fluctuations may not be able to bend a stiff polymer like actin which is grafted normal to the wall to permit intercalation. On the other hand, a filament polymerizing freely parallel to the

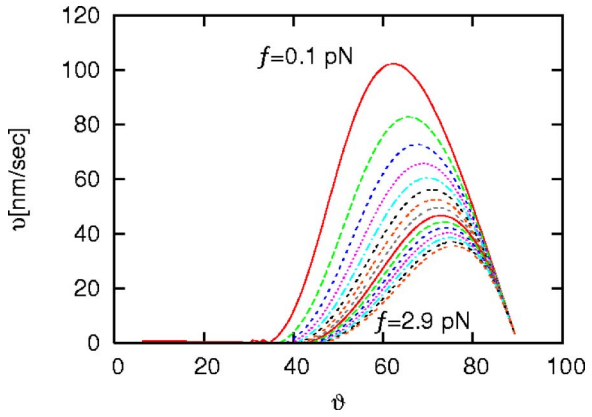

FIG. 20. (Color online) Growth velocity v versus graft angle ϑ (in degrees) for different load forces $f = 0.1$ pN, ..., 2.9 pN with steps 0.2 pN obtained using full expressions. Parameters are $L = 30$ nm, $l_p = 15$ μm, $k_{on}M = 110$ s^{-1}, and $k_{off} = 1$ s^{-1}.

wall is not able to exert force. In general, ϑ_{opt} is an increasing function of the load force and the persistence length. For the parameters listed in Fig. 20, this angle ranges from $\vartheta_{opt} \approx 60°$ at 0.1 pN to $\vartheta_{opt} \approx 75°$ at 2.9 pN. If the persistence length is lowered to $l_p \approx 1$ μm, the optimal angle is considerably decreased; compare Fig. 21(a).

For completeness, we have also included a plot for the protrusion velocity generated using the factorization approximation for all angles. We find qualitatively the same behavior as for the full expression but significant quantitative differences [see Fig. 21(b)].

VI. SUMMARY AND CONCLUSIONS

In summary, we have presented analytical calculations and extensive Monte Carlo simulations for the entropic force f exerted by a grafted polymer on a rigid obstacle (wall). The scale for the magnitude of the entropic force is given by the *Euler buckling force* $f_c \propto k_B T \ell_p / L^2$. The *stiffness parameter* $\varepsilon = L/\ell_p$ discerns the two universal regimes of a Gaussian chain ($\varepsilon \gg 1$) and a semiflexible chain ($\varepsilon \ll 1$). In this paper, we have mainly focused on the *stiff limit*, where analytical calculations using a weakly bending rod approximation are possible. In comparing our results with Monte Carlo simulations, we have found that the range of applicability of the results obtained in the stiff limit extend to stiffness parameters as large as $\varepsilon = 0.1$. Qualitatively the asymptotic results remain valid even up to $\varepsilon = 1$.

For the simplest possible geometry, where the polymer is perpendicular to the wall, located at a distance ζ from the grafted end, our analytical calculations show that the entropic force obeys a scaling law in the stiff limit

$$f_\parallel(\zeta, L, \ell_p) = f_c \tilde{f}_\parallel(\tilde{\eta}) \tag{101}$$

with the scaling variable $\tilde{\eta} = (L - \zeta)/L_\parallel$ measuring the minimal compression of the filament in units of the longitudinal width of the tip distribution function $L_\parallel = L^2/\ell_p$, and f_c the Euler buckling force of a classical beam. For small values of the scaling variable we have derived a simple analytical expression, (45),

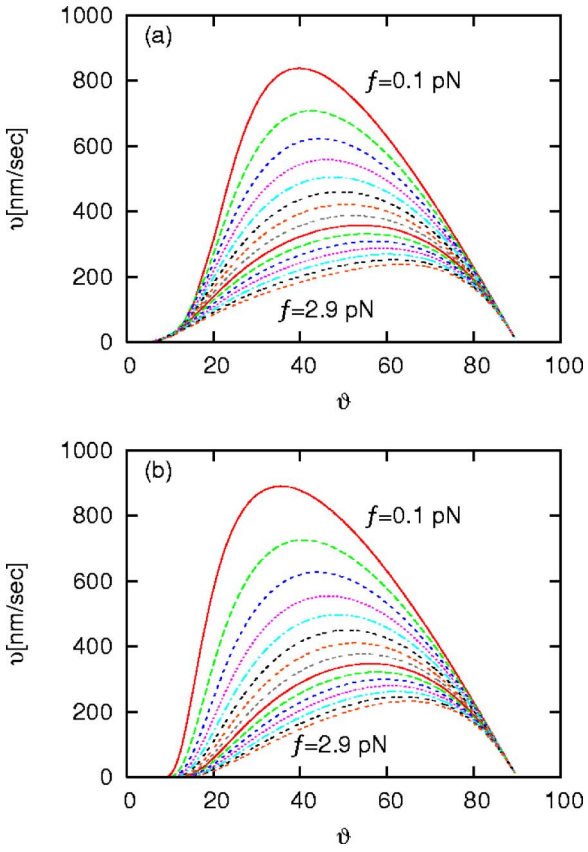

FIG. 21. (Color online) Protrusion velocity v versus inclination angle ϑ (in degrees) for different load forces $f=0.1$ pN, …, 2.9 pN with steps 0.2 pN obtained using (a) full expressions and (b) factorization approximation. Parameters are the same as in Ref. [7]: $L=30$ nm, $l_p=1$ μm, $k_{on}M=110$ s^{-1}, and $k_{off}=1$ s^{-1}.

$$\tilde{f}_{\parallel}^{<}(\tilde{\eta}) = \frac{4}{\pi^{5/2}} \frac{\exp(-1/4\,\tilde{\eta})}{\tilde{\eta}^{3/2}[1-2\,\mathrm{erfc}(1/2\sqrt{\tilde{\eta}})]} \tag{102}$$

and a corresponding formula in 2D, (58), which describe the full scaling function to a high numerical accuracy for $\tilde{\eta} \leqslant 0.2$. For $\tilde{\eta} \geqslant 0.2$, there are equally simple expressions, as for example (46) for 3D. We expect these formulas to be useful for molecular models of cell motility. The shape of the scaling function shows dramatic differences between 2D and 3D, which are of geometric origin. In 3D the entropic forces always stay below the Euler buckling force. In contrast, in 2D it is larger than the mechanical limit for most of the parameter space and exhibits a pronounced maximum at small values of the scaling variable $\tilde{\eta}$ before it steeply drops to zero as $\zeta \to L$.

Extensive Monte Carlo simulations confirm these analytical results and show that their range of applicability is $\varepsilon \leqslant 0.1$. For larger values of the stiffness parameter, there are clear deviations from the stiff scaling limit, which become qualitative for $\epsilon \geqslant 1$. Features of the stiff limit, such as the maximum in the entropic force, are visible even for ε as large as 4.

Experimentally, one should be able to measure entropic forces in 2D and compare it to 3D. For example, 2D force measurements may be feasible by confining the filament to fluctuate between two parallel plates. Since in some important biological systems like the leading edge of a crawling cell, the system is effectively 2D, these kind of experiments might also help to understand better a complex system like a lamellipodium.

For a polymer inclined at an angle ϑ with respect to the wall, the transverse width $L_\perp = \sqrt{L^3/3\ell_p}$ of the tip distribution function plays also a significant role; note that the ratio $L_\parallel/L_\perp = \sqrt{3\varepsilon}$. The entropic force can now be written in the scaling form

$$f(\zeta, \vartheta; L, \ell_p) = f_c(\vartheta)\tilde{f}(\eta_\parallel, \eta_\perp), \tag{103}$$

where $\eta_\perp = (L\cos\vartheta - \zeta)/(L_\perp \sin\vartheta)$, $\eta_\parallel = (L\cos\vartheta - \zeta)/\times(L_\parallel \cos\vartheta)$ and $f_c(\vartheta) = f_c/\cos\vartheta$. It turned out that a proper choice of scaling variables are $\mu = \eta_\parallel/\eta_\perp = (L_\perp/L_\parallel)\tan\vartheta$ and $\eta_\parallel$ or $\eta_\perp$ depending on whether the inclination angle is smaller or larger than a characteristic angle $\tan\vartheta_c = L_\parallel/L_\perp$, i.e., $\mu_c = 1$. Upon increasing the inclination parameter μ, the shape of the scaling function changes from a step-function-like form at $\mu = 0$ to a purely convex shape as $\mu \to \infty$. The limit $\mu \to \infty$ either corresponds to $\vartheta \to \pi/2$ or for a fixed $\vartheta \neq 0$ to the stiff limit $\varepsilon \to 0$. For 2D, in addition, the maximum vanishes at $\mu \approx 0.6$.

In the limit of inclination angles which are much larger than the characteristic angle ϑ_c, we have found that an approximation, (96) and (97), based on factorizing the joint probability distribution of the polymer tip gives an excellent asymptotic representation of the full analytical results:

$$f(\zeta, \vartheta) = \frac{k_B T}{L_\perp \sin\vartheta} \sqrt{\frac{2}{\pi}} \frac{e^{-\eta_\perp^2/2}}{\mathrm{erfc}(\eta_\perp/\sqrt{2})}. \tag{104}$$

It is simpler than the full scaling form since it only depends on one scaling variable. Up to minor factors this asymptotic formula for the entropic force is mathematically identical to the results found in Ref. [7], which was derived upon assuming that the tip of the polymer fluctuates perpendicular to its contour only. Since $\tan\vartheta_c \propto \sqrt{\varepsilon}$ the range of applicability of this results grows with increasing stiffness parameter. For example, ϑ_c equals approximately 30° and 10° for stiffness parameter ε equal to 0.1 and 0.006, respectively. For $\vartheta \leqslant \vartheta_c$ the factorization approximation fails completely, since it gives an incorrect description of the longitudinal stored length fluctuations. Then, a full analysis in terms of a two parameter scaling function is necessary.

We have finally shown that filaments in a polymerizing network grow fastest in a preferred direction ϑ_{opt}, such that one should expect that the population of those filaments growing near the optimal angle will be dominant. If the optimal angle ϑ_{opt} is larger that the critical angle ϑ_c, which is the case for an actin network with $l_p \approx 15$ μm, then one can to a large degree use the results from the factorization approximation.

ACKNOWLEDGMENTS

The authors acknowledge helpful discussions with Panayotis Benetatos, Martin Falcke, Thomas Franosch, Klaus Kroy, Gianluca Lattanzi, and Frederik Wagner. This work was supported by the Deutsche Forschungsgemeinschaft (Research Training Group 268 on "Dynamics and evolution of cellular and macromolecular processes").

APPENDIX A: INVERSE LAPLACE TRANSFORM OF THE MOMENT GENERATING FUNCTION

In this Appendix, we collect our calculations of the inverse Laplace transform of the moment generating functions. This will give two sets of series representations, which show good convergence properties either close to full stretching or for strong compression of the filament.

1. Series representation of the 3D tip distribution function for large stored length

Starting from the moment generating function $\mathcal{P}_\parallel(f)$, one can calculate the distribution function $P_\parallel(z)$ by an inverse Laplace, i.e., an integral along the imaginary axis,

$$P_\parallel(z) = \int_{-i\infty}^{+i\infty} \frac{df}{2\pi i} e^{f(L-z)} \mathcal{P}_\parallel(f). \tag{A1}$$

Since the moment generating function

$$\mathcal{P}_\parallel(f) = \prod_{k=1}^{\infty} \left(1 + \frac{4fL^2}{\ell_p (2k-1)^2 \pi^2}\right)^{-1} \tag{A2}$$

has poles at $f_k = -\lambda_k^2 \ell_p / L^2$ with $k = 1,2,3,\ldots$ only along the negative real axis, standard residuum calculus gives

$$\mathcal{P}_\parallel(f) = \sum_{k=1}^{\infty} \exp\left(-(L-z)\lambda_k^2 \frac{\ell_p}{L^2}\right) \times \prod_{l \neq k} \left(1 - \frac{(2k-1)^2}{(2l-1)^2}\right)^{-1} \left(\frac{L^2}{\ell_p \lambda_k^2}\right)^{-1}. \tag{A3}$$

Using $\Pi_{k=1}^{\infty}\left(1 - \frac{x^2}{(2k-1)^2}\right) = \cos\left(\frac{\pi}{2}x\right)$ [21], the product term can be written as

$$\begin{aligned} &\prod_{l \neq k} \left(1 - \frac{(2k-1)^2}{(2l-1)^2}\right)^{-1} \\ &= \lim_{k' \to k} \left(1 - \frac{(2k'-1)^2}{(2k-1)^2}\right) \prod_l \left(1 - \frac{(2k'-1)^2}{(2l-1)^2}\right)^{-1} \\ &= \lim_{k' \to k} \left(1 - \frac{(2k'-1)^2}{(2k-1)^2}\right) \cos^{-1}\left(\frac{\pi}{2}(2k'-1)\right) \\ &= 2\frac{(-1)^{k+1}}{\pi} \frac{2}{2k-1} = 2(-1)^{k+1} \frac{1}{\lambda_k}. \end{aligned} \tag{A4}$$

Hence we find

$$P_\parallel(z) = 2L_\parallel^{-1} \sum_{k=1}^{\infty} (-1)^{k+1} \lambda_k \exp[-\lambda_k^2 (L-z)/L_\parallel] \tag{A5}$$

with the characteristic longitudinal length scale $L_\parallel = L^2/\ell_p$.

2. Series representation for the tip distribution function close to full stretching: general *d*

We begin the analysis with the two-dimensional case, where

$$\mathcal{P}_\parallel(f) = \prod_{k=1}^{\infty} \left(1 + \frac{fL_\parallel}{\lambda_k^2}\right)^{-1/2} = \sqrt{\frac{1}{\cosh \sqrt{fL_\parallel}}}. \tag{A6}$$

For the derivation of our first series representation, we start from the product formula for the moment generating function. In this representation, one has branch cuts on the negative real axis at $\tilde{f} = fL_\parallel = -\lambda_k^2$ for $k \in \mathbb{N}$. We now deform the contour in the complex plane such that we enclose the negative real axis. Then

$$\begin{aligned} \tilde{P}_\parallel(\tilde{\rho}) &= \int_{-i\infty}^{+i\infty} \frac{d\tilde{f}}{2\pi i} e^{\tilde{f}\tilde{\rho}} \tilde{\mathcal{P}}_\parallel(\tilde{f}) \\ &= \int_{-\infty}^{0} \frac{d\tilde{f}}{2\pi i} e^{\tilde{f}\tilde{\rho}} \tilde{\mathcal{P}}_\parallel(\tilde{f} - i\epsilon) + \int_{0}^{-\infty} \frac{d\tilde{f}}{2\pi i} e^{\tilde{f}\tilde{\rho}} \tilde{\mathcal{P}}_\parallel(\tilde{f} + i\epsilon) \\ &= \int_{0}^{\infty} \frac{d\tilde{f}}{2\pi i} e^{-\tilde{f}\tilde{\rho}} [\tilde{\mathcal{P}}_\parallel(-\tilde{f} - i\epsilon) - \tilde{\mathcal{P}}_\parallel(-\tilde{f} + i\epsilon)], \end{aligned} \tag{A7}$$

where $\epsilon \to 0$. To proceed, we need to evaluate the product formula on the negative real axis. We find for $x \in (2k+1, 2k+3)\frac{\pi}{2}$,

$$\lim_{\epsilon \to 0} \prod_{l=1}^{\infty} \sqrt{1 - \frac{x^2 \mp i\epsilon}{\lambda_l^2}} = (\mp i)^k \frac{1}{\sqrt{|\cos x|}}. \tag{A8}$$

Upon substituting $y^2 = \tilde{f}$, this finally results in the series expansion

$$\tilde{P}_\parallel(\tilde{\rho}) = \frac{2}{\pi} \sum_{n=0}^{\infty} (-1)^n \int_{\lambda_{2n+1}}^{\lambda_{2n+2}} dy \frac{y e^{-y^2\tilde{\rho}}}{\sqrt{|\cos y|}}. \tag{A9}$$

For large values of $\tilde{\rho}$, corresponding to a significant compression of the polymer, the integral is dominated by the contribution from the interval $(\pi/2, 3\pi/2)$, such that the leading factor will be proportional to $\exp(-\pi^2\tilde{\rho}/4)$. In order to evaluate $\tilde{P}_\parallel(\tilde{\rho})$ further, we may average $y e^{-y^2\tilde{\rho}}$ over the interval and approximate the integral as

$$\int_{\lambda_{2n+1}}^{\lambda_{2n+2}} dy \frac{y e^{-y^2\tilde{\rho}}}{\sqrt{|\cos y|}} \approx \frac{1}{5} \sum_{m=4}^{8} \lambda_{2n+(m/4)} \exp(-\lambda_{2n+(m/4)}^2 \tilde{\rho}) \times \int_{\pi/2}^{3\pi/2} \frac{dy}{\sqrt{|\cos y|}} \tag{A10}$$

such that we finally get

$$\tilde{P}_\parallel(\tilde{\rho}) \approx \frac{1}{\mathcal{N}} \sum_{n=0}^{\infty} (-1)^n \sum_{m=4}^{8} \lambda_{2n+(m/4)} \exp(-\lambda_{2n+(m/4)}^2 \tilde{\rho}), \tag{A11}$$

where

$$\mathcal{N}^{-1} = \frac{2}{5\pi}\int_{\pi/2}^{3\pi/2} \frac{dy}{\sqrt{|\cos y|}} \approx 0.67. \tag{A12}$$

Next we drive a series representation suitable for small values of $\tilde{\rho}$. We use that for $f \in \mathbb{R}_+$ one has [22]

$$\mathcal{P}_\parallel(f) = \frac{1}{\sqrt{\cosh\sqrt{fL_\parallel}}}. \tag{A13}$$

With $\cosh(x)=\frac{1}{2}(e^x+e^{-x})$ and the generalized binomial theorem, this can be expanded to give

$$\mathcal{P}_\parallel(f) = \sqrt{2}\sum_{l=0}^{\infty}\binom{-\frac{1}{2}}{l} e^{-(2l+1/2)\sqrt{fL_\parallel}}, \tag{A14}$$

which is a holomorphic function on $\mathbb{C}\backslash\mathbb{R}_-$. Hence by the theorem of identity from complex calculus this formula remains valid $\forall f \in \mathbb{C}\backslash\mathbb{R}_-$. Substituting $y=\sqrt{fL_\parallel}$ transforms (A1) to

$$\tilde{P}_\parallel(\tilde{\rho}) = \int_{-i\infty+\varepsilon}^{i\infty+\varepsilon} \frac{dy}{\pi i} e^{y^2\tilde{\rho}} y \tilde{\mathcal{P}}_\parallel(y^2). \tag{A15}$$

Inserting the series representation (A14) and using the integral representation

$$D_1(z) = \sqrt{2\pi}e^{z^2/4}\int_{-i\infty+\varepsilon}^{i\infty+\varepsilon}\frac{ds}{2\pi i} s \exp\left(-zs+\frac{s^2}{2}\right) \tag{A16}$$

for the parabolic cylinder function [21] as well as

$$\binom{-\frac{1}{2}}{l} = (-1)^l \frac{(2l-1)!!}{2^l l!}, \tag{A17}$$

where $n!!=n(n-2)(n-4)\cdots$ yields

$$\tilde{P}_\parallel(\tilde{\rho}) = \frac{1}{\sqrt{\pi\tilde{\rho}}}\sum_{l=0}^{\infty}(-1)^l\frac{(2l-1)!!}{2^l l!} \times \exp\left(-\frac{\left(l+\frac{1}{4}\right)^2}{2\tilde{\rho}}\right) D_1\left(\frac{2l+\frac{1}{2}}{\sqrt{2\tilde{\rho}}}\right). \tag{A18}$$

With $D_1(x)=xe^{-x^2/4}$ (A18) becomes (50).

Finally, all the calculations are easily generalized to general spatial dimensions d. One finds the series representation

$$\tilde{P}_\parallel(\tilde{\rho}) = 2^{d/2}\frac{1}{\sqrt{2\pi}}\sum_{l=0}^{\infty}\binom{-\frac{1}{2}(d-1)}{l}\frac{l+\frac{1}{4}(d-1)}{\tilde{\rho}^{3/2}} \times\exp\left(-\frac{\left(l+\frac{d-1}{4}\right)^2}{\tilde{\rho}}\right) \tag{A19}$$

which is the fast converging for small $\tilde{\rho}$.

APPENDIX B: SADDLE POINT APPROXIMATION

Starting from (A1) and introducing $\tilde{f}=fL_\parallel$ gives

$$P_\parallel(z) = \int_{-i\infty}^{+i\infty}\frac{df}{2\pi i}e^{fL_\parallel\tilde{\rho}}\cosh^{-1}\sqrt{fL_\parallel} = L_\parallel^{-1}\int_{-i\infty}^{+i\infty}\frac{d\tilde{f}}{2\pi i}\frac{2e^{\tilde{f}\tilde{\rho}}}{e^{\sqrt{\tilde{f}}}+e^{-\sqrt{\tilde{f}}}}. \tag{B1}$$

We are interested to the asymptotic result of the integral close to full stretching $\tilde{\rho}\to 0$. Upon substituting $\tilde{f}=\xi/\tilde{\rho}^2$ one finds

$$P_\parallel(z) = \frac{2}{\tilde{\rho}^2 L_\parallel}\int_{-i\infty}^{+i\infty} d\xi \frac{\exp[f(\xi)/\tilde{\rho}]}{1+\exp(-2\sqrt{\xi}/\tilde{\rho})}, \tag{B2}$$

where $f(\xi)=\xi-\sqrt{\xi}$. Since the function $f(\xi)$ has a global maximum at $\xi_0=0.25$, the main contribution to the integral in the limit $1/\tilde{\rho}\to\infty$ comes from the integration along the curve of steepest descent which passes through ξ_0. We need to find this curve such that $\mathrm{Im}[f(\xi)]=\text{constant}=\mathrm{Im}[f(\xi_0)]=0$. We write $\sqrt{\xi}=\sqrt{a}(1+is)$ in terms of the curve parameter s. Then the condition $\mathrm{Im}[f(\xi_0)]=0$ gives $a=1/4$, and the curve of steepest descent is given in terms of $\mathrm{Re}[\xi]=\frac{1}{4}(1-s^2)$ and $\mathrm{Im}[\xi]=2as$, which is a parabola parametrized by s. The saddle point approximation amounts to a contour integral along this parabola, where $f(\xi)=-(1+s^2)/4$, such that

$$P_\parallel(z) = \frac{1}{L_\parallel\tilde{\rho}^2}\int_{-\infty}^{\infty}\frac{ds}{2\pi}(1+is)\frac{e^{-(1+s^2)/4\tilde{\rho}}}{1+e^{-(1+is)/\tilde{\rho}}}. \tag{B3}$$

To the leading order in $\tilde{\rho}$ we get

$$P_\parallel(z) = \frac{\exp(-1/4\tilde{\rho})}{\tilde{\rho}^2 L_\parallel}\int_{-\infty}^{+\infty}\frac{ds}{2\pi}\exp\left(\frac{-s^2}{4\tilde{\rho}}\right) = \frac{1}{\sqrt{\pi\tilde{\rho}^3}L_\parallel}\exp\left(-\frac{1}{4\tilde{\rho}}\right). \tag{B4}$$

In the two-dimensional case (2D), using the same strategy and substituting $\tilde{f}=\xi/\tilde{\rho}^{4/3}$ gives

$$P_\parallel(z) = \frac{1}{\sqrt{8\pi\tilde{\rho}^3}L_\parallel}\exp\left(-\frac{1}{16\tilde{\rho}}\right). \tag{B5}$$

APPENDIX C: JACOBI TRANSFORMATION OF THE RESTRICTED PARTITION SUM $\mathcal{Z}_\parallel(\zeta)$

To unclutter the formulas in this section, we use the generic argument x with $x\equiv\eta_\parallel$. $\mathcal{Z}_\parallel(x)$ can be written as

$$\tilde{\mathcal{Z}}_\parallel(x) = 2\int_0^\infty dy\sum_{k=-\infty}^{\infty}(-1)^{k+1}\delta(y-\lambda_k)\frac{1}{y}e^{-\ell_p y^2 x} = 2\int_0^\infty dy\,\tilde{\delta}(y)\frac{1}{y}e^{-\ell_p y^2 x} \tag{C1}$$

where we defined

$$\tilde{\delta}(y) := \sum_{k=-\infty}^{\infty}(-1)^{k+1}\delta(\lambda_k - y). \tag{C2}$$

Since $\tilde{\delta}(y)$ is odd in y and has periodicity 2π, we can expand it into a Fourier sine series,

$$\tilde{\delta}(y) = \sum_{l=1}^{\infty} d_l \sin(ly), \tag{C3}$$

where

$$d_l = \frac{2}{\pi}\int_0^{\pi} dy\,\tilde{\delta}(y)\sin(ly) = \frac{2}{\pi}\sin(l\pi/2) = \frac{2}{\pi}\begin{cases} 0 & \text{if } l \text{ is even,} \\ (-1)^{(l-1)/2} & \text{if } l \text{ is odd.} \end{cases} \tag{C4}$$

This results in

$$\tilde{\delta}(y) = \frac{2}{\pi}\sum_{l=1}^{\infty}(-1)^{l+1}\sin[(2l-1)y]. \tag{C5}$$

Inserting this into (C1) we find for $\mathcal{Z}_{\parallel}(x)$,

$$\tilde{\mathcal{Z}}_{\parallel}(x) = \frac{4}{\pi}\sum_{l=1}^{\infty}(-1)^{l+1}\int_0^{\infty} dy y^{-1}e^{-y^2x}\sin[(2l-1)y]. \tag{C6}$$

The integral evaluates to (21) (with $\mu=0$, $\beta=x$, $\gamma=2l-1$)

$$\int_0^{\infty} dy y^{-1}e^{-y^2x}\sin[(2l-1)y] = \frac{(2l-1)e^{-(2l-1)^2/4x}}{2\sqrt{x}}\sqrt{\pi}\,{}_1F_1\left(1;\frac{3}{2};\frac{(2l-1)^2}{4x}\right). \tag{C7}$$

As the confluent hypergeometric function ${}_1F_1(\alpha;\gamma;z) \equiv \Phi(\alpha,\gamma;z)$ has the property $\Phi(\alpha;\gamma;z)=e^z\Phi(\gamma-\alpha,\gamma;-z)$ [21] we find with Ref. [21]

$$\Phi\left(1,\frac{3}{2};z\right) = e^z\Phi\left(\frac{1}{2},\frac{3}{2};-z\right) = \frac{\sqrt{\pi}e^z}{2\sqrt{z}}\,\mathrm{erf}\,\sqrt{z}. \tag{C8}$$

Our result for $\mathcal{Z}_{\parallel}(x)$ is thus

$$\tilde{\mathcal{Z}}_{\parallel}(x) = 2\sum_{l=1}^{\infty}(-1)^{l+1}\,\mathrm{erf}\,\frac{2l-1}{2\sqrt{x}}. \tag{C9}$$

This still has problems for $x\to 0$ where $\mathrm{erf}[(2l-1)/2\sqrt{x}] \to 1$. We can, however rewrite it to

$$\tilde{\mathcal{Z}}_{\parallel}(x) = 2\sum_{l=1}^{\infty}(-1)^{l+1} + 2\sum_{l=1}^{\infty}(-1)^{l}\,\mathrm{erfc}\,\frac{2l-1}{2\sqrt{x}}. \tag{C10}$$

All convergence problems are now isolated in the first sum. As we know that $\mathcal{Z}_{\parallel}(0)=1$ [compare (36)] we assign $2\Sigma_{l=1}^{\infty}(-1)^{l+1}=1$ to finally find

$$\tilde{\mathcal{Z}}_{\parallel}(x) = 1 + 2\sum_{l=1}^{\infty}(-1)^{l}\,\mathrm{erfc}\,\frac{2l-1}{2\sqrt{x}}. \tag{C11}$$

APPENDIX D: GRAFT-ANGLE-DEPENDENT FORCE

We evaluate the general expression (60) using the representation

$$\Theta(x) = \lim_{\varepsilon\to 0+}\int\frac{dq}{2\pi i}\frac{e^{iqx}}{q-i\varepsilon} \tag{D1}$$

of the step function $\Theta(x)$. With (73) we find

$$\begin{aligned}\mathcal{Z}(\zeta,\vartheta) &= \int\frac{dq}{2\pi i}\frac{\exp\left(iq\dfrac{\zeta/\cos\vartheta - L}{L_{\parallel}}\right)}{q-i\varepsilon} \\ &\quad\times\int d\tilde{x}d\tilde{\eta}e^{iq\tilde{\eta}}e^{-iq(L_{\perp}/L_{\parallel})\tan\vartheta\tilde{x}}\tilde{P}(\tilde{x},\tilde{\eta}) \\ &= \int\frac{dq}{2\pi i}\frac{\exp\left(iq\dfrac{\zeta/\cos\vartheta - L}{L_{\parallel}}\right)}{q-i\varepsilon}a_d(-iq) \\ &\quad\times\exp[-(qL_{\perp}L_{\parallel}^{-1}\tan\vartheta)^2 3b(-iq)/2] \\ &= \tilde{\mathcal{Z}}\left(\frac{L-\zeta/\cos\vartheta}{L_{\parallel}},\frac{L_{\perp}}{L_{\parallel}}\tan\vartheta\right),\end{aligned} \tag{D2}$$

where

$$\tilde{\mathcal{Z}}(\eta_{\parallel},\mu) = -\int\frac{dq}{2\pi i}\frac{e^{iq}}{q+i\varepsilon}a_d(iq)e^{-3\mu^2q^2b(iq)/2}. \tag{D3}$$

Using the Dirac formula

$$\frac{1}{q+i\varepsilon} = \mathrm{P}:\frac{1}{q} - i\pi\delta(q), \tag{D4}$$

$a_3(0)=1$, $3b(0)=1$ and the symmetry properties of $a_3(iq)$ and $b(iq)$, we find

$$\tilde{\mathcal{Z}}(\eta_{\parallel},\mu) = \frac{1}{2} - 2\int_0^{\infty}\frac{dq}{2\pi}\frac{1}{q}\,\mathrm{Im}[e^{iq\eta_{\parallel}}a_3(iq)e^{-(1/2)\mu^2q^2 3b(iq)}]. \tag{D5}$$

The notation P denoting the principal value has been dropped as the integrand is regular at $q=0$. For large μ and/or ζ, $\tilde{\mathcal{Z}}(\eta_{\parallel},\mu)$ vanishes. This means that the integral in (85) must approach 1/2. Subtracting the result of numerically evaluating the nonvanishing integral from 1/2 strongly amplifies the unavoidable round-off error. We therefore rewrite (D5) to

$$\begin{aligned}\tilde{\mathcal{Z}}(\eta_{\parallel},\mu) &= \frac{1}{2}\mathrm{erfc}\frac{\eta_{\parallel}}{\sqrt{2}\mu} - 2\int_0^{\infty}\frac{dq}{2\pi}\frac{1}{q}\,\mathrm{Im}\{e^{iq\eta_{\parallel}} \\ &\quad\times[a_3(iq)e^{-(1/2)\mu^2q^2 3b(iq)} - e^{-(\mu^2q^2)/2}]\},\end{aligned} \tag{D6}$$

where we used the identity

$$\frac{1}{2} - \mathrm{P}:\int_{-\infty}^{\infty}\frac{dq}{2\pi i}\frac{e^{iq\eta_{\parallel}}}{q}e^{-(q^2\mu^2)/2} = \frac{1}{2}\mathrm{erfc}\frac{\eta_{\parallel}}{\sqrt{2}\mu}. \tag{D7}$$

As $\mathrm{Im}\,q^2b(iq)\sim -q$ for large $|q|$, it is again advantageous to split the integrals at some q_0 and, for $q>q_0$, to rewrite the imaginary part appearing in the integrand of (D6) to

$$\mathrm{Im}\{e^{iq(\eta_\parallel+3\mu^2/2)}[a_3(iq)e^{-(3/2)\mu^2[q^2b(iq)+iq]}-e^{-(\mu^2q^2+3iq\mu^2)/2}]\} \tag{D8}$$

and the real part appearing in (89) to

$$\mathrm{Re}[e^{iq(\eta_\parallel+3\mu^2/2)}a_3(iq)e^{-(3/2)\mu^2[q^2b(iq)+iq]}]. \tag{D9}$$

In both cases, the integrand is holomorphic for $\mathrm{Im}\, q<0$. Hence the integrals vanish if $\delta\eta_\parallel := \eta_\parallel+\mu^2/2<0$ which we already understood in the simple geometric picture of the problem.

Both integrals now vanish in the limit of large $\eta_\parallel$ and have well-behaved integrands on $[0,\infty]$. The precision with which $\tilde{f}(\eta_\parallel,\mu)$ can be calculated is, however, still limited by the relative error in evaluating the integrals. This relative error grows quickly with increasing $\eta_\parallel$ limiting the range of $\eta_\parallel$ over which $\tilde{f}(\eta_\parallel,\mu)$ can be calculated reliably [note that the first term of (D6) vanishes with increasing $\eta_\parallel$ as well].

[1] W. Helfrich, Z. Naturforsch. A **33A**, 305 (1978).
[2] M. Fixman and J. Kovac, J. Chem. Phys. **58**, 1564 (1973); J. Kovac and C. C. Crabb, Macromolecules **15**, 537 (1982); J. F. Marko and E. Siggia, *ibid.* **28**, 209 (1995).
[3] P. Benetatos and E. Frey, Phys. Rev. E **70**, 051806 (2004).
[4] See recent work by Y. Marcy *et al.*, Proc. Natl. Acad. Sci. U.S.A. **101**, 5992 (2004) and references cited therein.
[5] D. Bray, *Cell Movements* (Garland, New York, 2001).
[6] F. Gerbal, P. Chaikin, Y. Rabin, and J. Prost, Biophys. J. **79**, 2259 (2000).
[7] A. Mogilner and G. Oster, Biophys. J. **71**, 3030 (1996).
[8] A. Mogilner and G. Oster, Eur. Biophys. J. **25**, 47 (1996).
[9] L. LeGoff, O. Hallatschek, E. Frey, and F. Amblard, Phys. Rev. Lett. **89**, 258101 (2002).
[10] F. Pampaloni, G. Lattanzi, A. Jonas, T. Surrey, E. Frey, and E.-L. Florin, Proc. Natl. Acad. Sci. U.S.A. **103**, 10248 (2006).
[11] J. V. Small, M. Herzog, and K. Anderson, J. Cell Biol. **129**, 1275 (1995).
[12] O. Kratky and G. Porod, Recl. Trav. Chim. Pays-Bas **68**, 1106 (1949).
[13] N. Saito, K. Takahashi, and Y. Yunoki, J. Phys. Soc. Jpn. **22**, 219 (1967).
[14] J. Wilhelm and E. Frey, Phys. Rev. Lett. **77**, 2581 (1996).
[15] E. Frey, K. Kroy, J. Wilhelm, and E. Sackmann, in *Dynamical Networks in Physics and Biology*, edited by D. Beysens and G. Forgacs (Springer, Berlin, 1998).
[16] Actually, one must be slightly more precise and say that one considers a case where the obstacle is fixed and rigid on time scales where the thermal fluctuations of the filament equilibrate.
[17] T. C. Lubensky, Solid State Commun. **102**, 187 (1997).
[18] R. Roth, R. van Roij, D. Andrienko, K. R. Mecke, and S. Dietrich, Phys. Rev. Lett. **89**, 088301 (2002).
[19] G. Lattanzi, T. Munk, and E. Frey, Phys. Rev. E **69**, 021801 (2004).
[20] P. Benetatos, T. Munk, and E. Frey, Phys. Rev. E **72**, 030801(R) (2005).
[21] A. Abramowitz and I. A. Stegun, *Handbook of Mathematical Functions with Formulas, Graphs, and Mathematical Tables* (Dover, New York, 1970).
[22] Eldon R. Hansen, *A Table of Series and Products* (Prentice-Hall, Englewood Cliffs, NJ, 1975).
[23] K. Kroy and E. Frey, Phys. Rev. Lett. **77**, 306 (1996).
[24] L. D. Landau and E. M. Lifshitz, *Theory of Elasticity* (Pergamon, London, 1959).
[25] F. Wagner, A. Gholami, G. Lattanzi, and E. Frey (unpublished).
[26] A. Gholami and E. Frey (unpublished).